Numerical Valuation of American Options under Exponential Lévy Processes

Xinzheng Huang

Delft Institute for Applied Mathematics
Delft University of Technology
Delft, the Netherlands

July, 2005

Supervisor: Dr. ir. Cornelis W. Oosterlee

MSc Committee : Prof. dr. Roger M. Cooke
Dr. ir. Cornelis W. Oosterlee
Dr. ir. J.A.M van der Weide

Preface

The valuation of American options is of practical importance because the majority of exchange-traded options are American. We focus on numerical issues related to American options since there are no closed form solutions available for American options. We investigate the option price, the optimal exercise boundary and the Greeks (partial derivatives of the option prices).

Two models for the dynamics of stock prices are considered: the Black-Scholes model and the variance gamma model. The Black-Scholes model, which marks the beginning of the modern era of financial derivatives and remains dominant in options trading, assumes that the log-price of stocks follows a geometric Brownian motion. The variance gamma model is a three parameter model that is obtained by evaluating a Brownian motion at random times given by a gamma process.

We present accurate numerical solutions for option prices with only a few grid points. Grid stretching in space by means of analytic coordinate transformations is implemented and high order accuracy is achieved. This stretching can be time-dependent so as to capture the optimal exercise boundary for American style options.

The thesis is organized as follows: Chapter 1 gives a brief introduction to the Black-Scholes framework for option pricing and the formulation of the American option as a free boundary problem. Chapter 2 introduces some elements of Lévy processes and generalizes the geometric Brownian motion model to an exponential Lévy model. Chapters 3 and 4 discuss issues of valuation of options under the Black-Scholes model and the variance gamma model, respectively.

I'd like to express my sincere appreciation to my thesis advisor Dr. Kees Oosterlee for offering me the opportunity to work on such exciting subjects and for his guidance and valuable comments. Thanks to Dr. Ariel Almendral and Coenraad Leentvaar for their generous support and helpful discussions.

I would also like to thank Dr. Hans van der Weide, who introduced me to the field of financial mathematics. I benefited a lot from his lectures and instructions.

I also owe a great debt of gratitude to Prof. Roger Cooke for his care, kindness and encouragement. I very much enjoyed my time at Delft.

Last but not least I thank my family for always supporting me.

Contents

List of Tables

List of Figures

Chapter 1

Introduction

1.1 Black-Scholes Framework

We assume a frictionless market that satisfies the no-arbitrage principle. We have a bank account $B = (B_t)_{t\geq 0}$ with constant interest rate r and stock $S = (S_t)_{t\geq 0}$ with expected rate of return on the stock μ and stock price volatility σ. Under the Black-Scholes framework, the dynamics of B and S are given respectively by

$$dB_t = rB_t dt, \tag{1.1}$$

$$dS_t = \mu S_t dt + \sigma S_t d\widetilde{W}_t, \tag{1.2}$$

where $\widetilde{W}_t$ is a standard Brownian motion on a probability space $(\Omega, \mathcal{F}, \mathbb{P})$.

Let $V(t, S)$ be the value of a European option with underlying asset S and terminal payoff $\Phi(S_T)$. Assuming that $V(t, S)$ has suitable differentiability properties (specifically $V(\cdot, \cdot) \in C^{1,2}$) , we can apply the Itô formula to $V(t, S)$ to get

$$dV = (\frac{\partial V}{\partial t} + \frac{1}{2}\sigma^2 S^2 \frac{\partial^2 V}{\partial S^2})dt + \frac{\partial V}{\partial S} dS_t. \tag{1.3}$$

It follows that we can construct an instantaneously risk free portfolio consisting of one option and $-\frac{\partial V}{\partial S}$ of the underlying asset. The value of the portfolio is

$$\pi = V - \frac{\partial V}{\partial S} S$$

with the dynamics

$$d\pi = (\frac{\partial V}{\partial t} + \frac{1}{2}\sigma^2 S^2 \frac{\partial^2 V}{\partial S^2})dt.$$

To avoid arbitrage the expected capital gain must equal $r\pi dt$. Then we reach the following Black-Scholes equation:

$$\frac{\partial V}{\partial t} + \frac{1}{2}\sigma^2 S^2 \frac{\partial^2 V}{\partial S^2} + rS\frac{\partial V}{\partial S} - rV = 0, \tag{1.4}$$

subject to the final condition $V(T, S_T) = \Phi(S_T)$ and some suitable boundary conditions.

By an application of the Feynman-Kac formula (see Øksendal [40]) we know the solution to (1.4) is given by

$$V(t,S) = e^{-r(T-t)}E^{\mathbb{Q}}[\Phi(S_T)|S_t = S], \tag{1.5}$$

where

(i) $\mathbb{Q}$ is a probability equivalent to $\mathbb{P}$, such that the discounted price $e^{-rt}V(t,S)$ is a $\mathbb{Q}$-martingale (therefore $\mathbb{Q}$ is called as equivalent martingale measure or risk neutral measure), and

(ii) with W_t being a Brownian motion on the probability space $(\Omega, \mathcal{F}, \mathbb{Q})$, S_T is given by

$$S_T = S_t e^{(r-\frac{\sigma^2}{2})(T-t)+\sigma(W_T-W_t)},$$

and the $\mathbb{Q}$-dynamics of S satisfies the equation

$$dS_t = rS_t dt + \sigma S_t dW_t, \tag{1.6}$$

We further note the partial derivative $\frac{\partial V}{\partial S}$, commonly referred to as Delta(Δ), is an important parameter in the pricing and hedging of options. It is a measure of the rate of change in the option price with respect to the price of the underlying asset. The Gamma(Γ) of an option, $\frac{\partial^2 V}{\partial S^2}$, is also of importance since it measures the rate of the change of the option's delta with respect to the price of the underlying asset.

1.2 American Options

In contrast to a European option, which can only be exercised on the maturity date T, an American option can be exercised at any time up to T. Consequently, identifying the optimal exercise strategy is an integral part of the valuation problem.

Let $V(t,S)$ be the value of an American option with payoff $\Phi(S)$ at exercise. The possibility of early exercise requires

$$V(t,S) \geq \Phi(S), \quad \forall\, t \in [0,T],$$

otherwise an arbitrage opportunity would arise.

The valuation of the American option is known as a free boundary problem. The free boundary $S_f(t)$, also called optimal exercise boundary or early exercise boundary, divides the (t,S) half strip into two parts, namely the continuation region and the stopping region. The continuation region $\{(t,S) \in [0,T] \times \mathbb{R}_+ : V(t,S) > \Phi(S)\}$ is the set of points (t,S) at which the option is worth more alive. While in the stopping region $\{(t,S) \in [0,T] \times \mathbb{R}_+ : V(t,S) = \Phi(S)\}$ early exercise is advisable.

Therefore under the Black-Scholes framework, the price $V(t,S)$ satisfies either in the continuation region

$$V(t,S) > \Phi(S), \quad \frac{\partial V}{\partial t} + \frac{1}{2}\sigma^2 S^2 \frac{\partial^2 V}{\partial S^2} + rS\frac{\partial V}{\partial S} - rV = 0;$$

or in the stopping region

$$V(t,S) = \Phi(S), \quad \frac{\partial V}{\partial t} + \frac{1}{2}\sigma^2 S^2 \frac{\partial^2 V}{\partial S^2} + rS\frac{\partial V}{\partial S} - rV < 0.$$

Additionally the boundary conditions at $S_f(t)$ are that V and $\frac{\partial V}{\partial S}$ are continuous at $S_f(t)$:

$$V(t,S_f(t)) = \Phi(S_f(t)), \quad \frac{\partial V(t,S_f(t))}{\partial S} = \Phi'(S_f(t)),$$

which is known as the *smooth fit principle*.

This leads to a *linear complementarity problem* formulated as follows

$$V(t,S) \geq \Phi(S), \tag{1.7}$$

$$-\Big(\frac{\partial V}{\partial t} + \frac{1}{2}\sigma^2 S^2 \frac{\partial^2 V}{\partial S^2} + rS\frac{\partial V}{\partial S} - rV\Big) \geq 0, \tag{1.8}$$

$$\Big(\frac{\partial V}{\partial t} + \frac{1}{2}\sigma^2 S^2 \frac{\partial^2 V}{\partial S^2} + rS\frac{\partial V}{\partial S} - rV\Big)\big(V(t,S) - \Phi(S)\big) = 0 \tag{1.9}$$

with some final and boundary conditions. Solutions of linear complementarity problems can be obtained by a variety of iterative methods, e.g., by the projected successive overrelaxation (PSOR) method we are going to use. The optimal exercise boundary $S_f(t)$ is automatically captured by this formulation.

1.3 Beyond the Black-Scholes Model

While the Black-Scholes model is popular in practice, its pitfalls are also well documented, see for instance Fama [23], Eberlein and Keller [21], Bakshi, Cao and Chen [7]. Empirical studies on asset returns suggest significant departures from the properties of geometric Brownian motion in the Black-Scholes model, e.g., leptokurtosis (high peak and fat tails) and skewness of the return distribution instead of the normality assumption. Evidence from the option market include (i) the volatility smile or skew, and (ii) the underpricing by the Black-Scholes formula for short term out-of-money options.

Among the many extensions to the Black-Scholes model to resolve these empirical biases, we concentrate on jump models in the sequel. Various jump processes have been proposed in finance to model the dynamics of asset returns. They can be divided into two types: (i) jump-diffusion models and (ii) pure jump processes. Merton's jump-diffusion model with Gaussian jumps [37] and Kou's model with double exponential jumps [31] are of the first type. Both are combinations of a Brownian motion and a compound Poisson process with some given distribution of the jump sizes. Examples of the second type include the normal inverse Gaussian (NIG) model of Barndorff-Nielsen [8], the generalized hyperbolic class of Eberlein, Keller, and Prause [22], the variance gamma (VG) model of Madan and Milne [35] and Madan, Carr and Chang [36], its generalization to the CGMY model of Carr, Geman, Madan and Yor [12], the finite moment log-stable (LS) model of Carr and Wu [14] and the Meixner model of Schoutens [44].

All the models mentioned above, together with the drifted Brownian motion in the Black-Scholes model, fall into the category of Lévy processes. In the next chapter, we

give the definition and some properties of Lévy processes. We also introduce two Lévy processes: Brownian motion and the variance gamma process. Finally, we generalize the Black-Scholes framework to exponential Lévy models and reach a partial integro-differential equation for the purpose of option pricing.

Chapter 2

Option Valuation under Exponential Lévy Processes

2.1 Lévy Processes

Let $X = (X_t)_{t\geq 0}$ be a stochastic process defined on a probability space $(\Omega, \mathcal{F}, \mathbb{P})$. We say that it has *independent increments* if for each $n \in N$ and each $0 \leq t_1 < t_2 < \cdots < t_{n+1} < \infty$ the random variables $(X_{t_{j+1}} - X_{t_j},\ 1 \leq j \leq n)$ are mutually independent and that it has *stationary increments* if each $X_{t_{j+1}} - X_{t_j}$ and $X_{t_{j+1}-t_j} - X_0$ have the same distribution.

Definition 1 (Lévy process) *$(X_t)_{t\geq 0}$ is a Lévy process if :*

(i) *$X_0 = 0$ $(a.s.)$;*

(ii) *X has independent and stationary increments;*

(iii) *X is stochastically continuous, i.e. for all $\varepsilon > 0$ and for all $s > 0$*

$$\lim_{t\to s} P(|X_t - X_s| > \varepsilon) = 0.$$

The law of a Lévy process is completely determined by its characteristic triplet $(\sigma^2, \upsilon, \gamma)$, where $\sigma^2 \in [0, \infty)$ is called Gaussian variance since it is associated with the Brownian motion, $\gamma \in \mathbb{R}$ is the drift term and Π is a *Lévy measure*, i.e., a Borel measure defined on $\mathbb{R}\backslash\{0\}$ which satisfies

$$\int_{\mathbb{R}} (|x|^2 \wedge 1)\Pi(dx) < \infty.$$

The characteristic function of X can be computed from the triplet as follows.

Theorem 1 (Lévy-Khintchine representation) *Let $(X_t)_{t\geq 0}$ be a Lévy process on $\mathbb{R}$ with characteristic triplet (σ^2, Π, γ). Then*

$$E[e^{izX_t}] = e^{t\Psi(z)},\ z \in \mathbb{R} \tag{2.1}$$

with

$$\Psi(z) = -\frac{\sigma^2}{2}z^2 + i\gamma z + \int_{\mathbb{R}}(e^{izx} - 1 - izx\mathbf{1}_{\{|x|\leq 1\}})\Pi(dx). \tag{2.2}$$

Definition 2 (Subordinator) *A subordinator is a one-dimensional Lévy process that is non-decreasing (a.s.).*

A subordinator thus must not have a diffusion component, but only positive jumps and a non-negative drift (see [15]). Let S_t be a subordinator with characteristic triplet $(0, \rho, b)$. The moment generating function of S_t is

$$E[e^{uS_t}] = e^{t\,l(u)} \quad \forall u \leq 0, \quad \textit{where } l(u) = bu + \int_0^\infty (e^{ux} - 1)\rho(dx). \tag{2.3}$$

The function $l(u)$ is usually called the *Laplace exponent* of the subordinator.

Example 1 (Gamma subordinator) *Let $G(t; \mu, \nu)$ be a gamma process with mean rate μ and variance rate ν. The density of the gamma process at time t is given by*

$$f(g) = \left(\frac{\mu}{\nu}\right)^{\frac{\mu^2 t}{\nu}} \frac{g^{\frac{\mu^2 t}{\nu}-1}\exp(-\frac{\mu}{\nu}g)}{\Gamma(\frac{\mu^2 t}{\nu})}, \; g \geq 0, \tag{2.4}$$

where $\Gamma(x)$ is the gamma function. Its moment generating function is given by

$$E[e^{uS_t}] = \left(\frac{1}{1 - u\frac{\nu}{\mu}}\right)^{\frac{\mu^2 t}{\nu}} \quad \textit{with Laplace exponent} \quad l(u) = -\frac{\mu^2}{\nu}\ln(1 - u\frac{\nu}{\mu}).$$

It is easy to verify

$$l(u) = \int_0^\infty (e^{ux} - 1)\frac{\mu^2 exp(-\frac{\mu}{\nu}x)}{\nu x}dx.$$

From this we see that $G(t)$ is a subordinator with $b = 0$ and $\rho(dx) = \frac{\mu^2 exp(-\frac{\mu}{\nu}x)}{\nu x}dx$.

Subordinators can be used for "time changing" other Lévy processes. An example called the variance gamma(VG) process will be presented later. Before that, we point out a key result regarding subordination.

Theorem 2 (Subordination of a Lévy process) *Let $(\Omega, \mathcal{F}, \mathbb{P})$ be a given probability space, X_t be a Lévy process on $\mathbb{R}$ with characteristic exponent $\Psi(u)$ and triplet (σ^2, Π, γ) and S_t be a subordinator with Laplace exponent $l(u)$ and characteristic triplet $(0, \rho, b)$. Assume X_t and S_t are independent, then the process Y_t defined for each $\omega \in \Omega$ by $Y(t, \omega) = X(S(t, \omega), \omega)$ is a Lévy process and its characteristic function is given by*

$$E[e^{iuY_t}] = e^{tl(\Psi(u))}. \tag{2.5}$$

The complete proof of Theorem 2 can be found in Applebaum[5]. We only show here that the formula (2.5) can be obtained by conditioning on $\mathcal{F}^{\mathcal{S}}$:

$$E[e^{iuX(S_t)}] = E\{\, E[e^{iuX(S_t)}|\mathcal{F}^{\mathcal{S}}]\,\} = E[e^{S_t\Psi(u)}] = e^{tl(\Psi(u))}.$$

2.2 Examples of Lévy Processes in Finance

The two models presented here are those we aim to solve numerically in later chapters. For properties of other Lévy processes such as the Lévy measures and characteristic exponents, see Schoutens [45].

2.2.1 Brownian Motion

The introduction of Brownian motion in finance can be traced back to Bachelier [6]. It is the process driving the log-price of an asset in Samuelson [43] and the celebrated Black-Scholes model.

Definition 3 (Brownian motion) *A (standard) Brownian motion in* $\mathbb{R}$ *is a Lévy process* $(W_t)_{t\geq 0}$ *for which*

(i) $W_0 = 0$ *(a.s.);*

(ii) $W_t \sim N(0,t)$ *for each* $t \geq 0$*;*

(iii) W *has continuous sample paths.*

It follows immediately that the characteristic triplet of a standard Brownian motion $(W_t)_{t\geq 0}$ is $(1,0,0)$.

A drifted Brownian motion b_t can be constructed by

$$b_t = \theta t + \sigma W_t; \tag{2.6}$$

Then b is a Lévy process with each $b_t \sim N(\theta t, \sigma^2 t)$. Its characteristic triplet is $(\sigma^2, 0, \theta)$.

We note that (drifted) Brownian motion is the only Lévy process with continuous sample paths and it is an infinite variation process.

2.2.2 The Variance Gamma Process

The variance gamma model was first introduced in Madan and Seneta [34] and extended by Madan, Carr and Chang [36]. We follow the later and Carr, Geman, Madan and Yor [12] very closely.

The VG process is a subordinated version of Brownian motion, in other words, it could be interpreted as a Brownian motion in "business time" instead of calender time. Let $b(t;\theta,\sigma) = \theta t + \sigma W(t)$, where $W(t)$ is a standard Brownian motion. Let $G(t;1,\nu)$ be a gamma process with mean rate unity and variance rate ν. Then the VG process is defined by

$$X(t;\sigma,\nu,\theta) = b(G(t;1,\nu);\theta,\sigma) = \theta G(t;1,\nu) + \sigma W(G(t;1,\nu)). \tag{2.7}$$

By an application of Theorem 2 we obtain its characteristic function as follows

$$\phi_{VG}(u,t) = E\{exp\,[iuX_{VG}(t)]\} = \Big(\frac{1}{1 - i\theta\nu u + \sigma^2\nu u^2/2}\Big)^{t/\nu}. \tag{2.8}$$

The VG process can also be regarded as the difference of two independent gamma processes. Observing that

$$\frac{1}{1-i\theta\nu u+\sigma^2\nu u^2/2}=(\frac{1}{1-i\eta_p u})(\frac{1}{1+i\eta_n u}),$$

where $\eta_p,\ \eta_n$ satisfy

$$\eta_p-\eta_n=\theta\nu \quad and \quad \eta_p\eta_n=\frac{\sigma^2\nu}{2}.$$

It follows that η_p and $-\eta_n$ are the roots of the equation

$$x^2-\theta\nu x-\sigma^2\nu/2=0,$$

whereby

$$\eta_p=\sqrt{\frac{\theta^2\nu^2}{4}+\frac{\sigma^2\nu}{2}}+\frac{\theta\nu}{2}, \quad and \quad \eta_n=\sqrt{\frac{\theta^2\nu^2}{4}+\frac{\sigma^2\nu}{2}}-\frac{\theta\nu}{2}$$

The two gamma processes may be denoted $G_p(t;\mu_p,\nu_p)$ and $G_n(t;\mu_n,\nu_n)$, with, respectively, mean and variance rates μ_p,μ_n and ν_p,ν_n. For these gamma processes, we have that $\mu_p=\eta_p/\nu,\mu_n=\eta_n/\nu$, while $\nu_p=\mu_p^2\nu$, and $\nu_n=\mu_n^2\nu$. We then have that

$$X_{VG}(t;\sigma,\nu,\theta)=G_p(t;\mu_p,\nu_p)-G_n(t;\mu_n,\nu_n). \tag{2.9}$$

and we may write the Lévy measure $\Pi(dx)$ for X_t as

$$\Pi_{VG}(dx)=\begin{cases}\dfrac{\mu_n^2}{\nu_n}\dfrac{exp(-\dfrac{\mu_n}{\nu_n}|x|)}{|x|}dx & \text{for } x<0\\[2ex] \dfrac{\mu_p^2}{\nu_p}\dfrac{exp(-\dfrac{\mu_p}{\nu_p}x)}{x}dx & \text{for } x>0\end{cases} \tag{2.10}$$

We could also define the Lévy measure in terms of the original parameters (σ,ν,θ) as

$$\Pi_{VG}(dx)=\frac{exp\,(\theta x/\sigma^2)}{\nu|x|}exp\left(-\frac{\sqrt{\frac{2}{\nu}+\frac{\theta^2}{\sigma^2}}}{\sigma}|x|\right)dx. \tag{2.11}$$

The parameters ν and θ play important roles in capturing the non normality of the asset returns. Clearly when $\theta<0$, negative values of x receive a higher relative probability than the corresponding positive values, which means that negative values of θ give rise to a negative skewness. Meanwhile large values of ν yields lower decay rate of the Lévy measure, and therefore raise tail probability and kurtosis.

The Lévy measure in (2.11) also tells us that the VG process is of infinite activity and finite variation since Π integrates to infinity on the real line and $|x|$ is integrable with respect to Π.[1] An infinite activity jump process has infinite number of jumps (mostly small) in any finite interval, which is versatile enough to include both small jumps to mimic a Brownian component and large jumps. Consequently, unlike the

[1]For more details on infinite activity Lévy processes and finite variation Lévy processes, see Cont and Tankov [15].

jump-diffusion model, a Brownian part is no longer necessary. Being of finite variation, the price process can be decomposed into the difference of two increasing processes representing the increase and decrease of the prices. Argued by Carr, Geman, Madan and Yor [12] following their empirical investigation, the statistical and risk-neutral processes for equity prices are pure jump processes of infinite activity and finite variation.

Finally, we would like to mention that the VG process is a special case of the so-called CGMY process. The CGMY Lévy density has 4 parameters C, G, M and Y and is given by

$$\Pi_{CGMY}(dx) = \begin{cases} C\frac{exp(-G|x|)}{|x|^{1+Y}}dx & \text{for } x < 0 \\ C\frac{exp(-M|x|)}{|x|^{1+Y}}dx & \text{for } x > 0 \end{cases} \tag{2.12}$$

where $C > 0,\ G \geq 0,\ M \geq 0$ and $Y < 2$. The VG process is the case where $Y = 0$, $C = 1/\nu$, $G = 1/\eta_n$ and $M = 1/\eta_p$.

2.3 Partial Integro-differential Equations

An exponential Lévy model is formulated by simply replacing the drifted Brownian motion in the Black-Scholes model of asset prices by a Lévy process:

$$S_t = S_0\, exp\,(X_t), \tag{2.13}$$

where X is a Lévy process with characteristic triplet $(\sigma^2, \widetilde{\Pi}, \widetilde{\gamma})$ under measure $\mathbb{P}$ and satisfies some integrability condition. From the perspective of no-arbitrage[2] there must exist an equivalent martingale measure $\mathbb{Q}$, under which X has the characteristic triplet (σ^2, Π, γ) and satisfies $E^{\mathbb{Q}}[exp\,(X_t)] = e^{rt}$, i.e., the expected return on stock S is the same as that from a money account. This amounts to

$$\frac{\sigma^2}{2} + \gamma + \int_{\mathbb{R}} (e^x - 1 - x\mathbf{1}_{\{|x|\leq 1\}})\Pi(dx) = r, \tag{2.14}$$

which is a consequence of Lévy-Khintchine formula.

In models with jumps the market is incomplete: there are many possible choices for the equivalent martingale measure. A convenient way to achieve the above change of measure is the Esscher transform, which is defined as follows.

Definition 4 (Esscher Transform) *Let X be a Lévy process on the probability space $(\Omega, \mathcal{F}, \mathbb{P})$. Then the Esscher transform is any change of $\mathbb{P}$ by the process X_t and a constant θ to an equivalent probability measure $\mathbb{Q}$ such that*

$$\frac{d\mathbb{Q}}{d\mathbb{P}}\Big|\mathcal{F}_t = \frac{exp(\theta X_t)}{E[exp(\theta X_t)]}. \tag{2.15}$$

[2]More precisely, No Free Lunch with Vanishing Risk(NFLVR), see Delbaen and Schachermayer [19, 20].

If such an Esscher transformed martingale measure $\mathbb{Q}$ exists, we should have $\gamma = \widetilde{\gamma} + \theta\sigma^2 + \int_{-1}^{1} x(e^{\theta x} - 1)\Pi(dx)$, and $\Pi(dx) = e^{\theta x}\widetilde{\Pi}(dx)$. For more details on Esscher transforms, see Gerber and Liu [25].

Let $V(t, S)$ again be the value of a European option with underlying asset S and terminal payoff $\Phi(S_T)$. Under risk neutral probability $\mathbb{Q}$, we have

$$V(t, S) = e^{-r(T-t)}E^{\mathbb{Q}}[\Phi(S_T)|S_t = S] = e^{-r(T-t)}E^{\mathbb{Q}}[\Phi(Se^{X_{T-t}})]. \tag{2.16}$$

Making the change of variables $x = \ln S$ and $\tau = T - t$, we define

$$u(\tau, x) = V(t, S) = e^{-r\tau}E^{\mathbb{Q}}[\Phi(e^{x+X_\tau})]$$

and differentiate $u(\tau, x)$ with respect to τ to obtain the following partial integro-differential equation(PIDE):

$$\frac{\partial u}{\partial \tau} = Lu(x), \tag{2.17}$$

where the operator L is defined by the following proposition.

Proposition 1 (Infinitesimal generator of a Lévy process) *Let $(X_t)_{t\geq 0}$ be a Lévy process on $\mathbb{R}$ with characteristic triplet (σ^2, Π, γ). Then the infinitesimal generator of X is defined for any $f \in C_0^2(\mathbb{R})$ as*

$$Lf(x) = \frac{1}{2}\sigma^2\frac{\partial^2 f}{\partial x^2}(x) + \gamma\frac{\partial f}{\partial x}(x) + \int_{\mathbb{R}}\Big(f(x+y) - f(x) - y\frac{\partial f}{\partial x}(x)\mathbf{1}_{\{|y|\leq 1\}}\Big)\Pi(dy), \tag{2.18}$$

where $C_0^2(\mathbb{R})$ is the set of twice continuously differentiable functions, vanishing at infinity.

By further applying condition (2.14) we come to the following PIDE:

$$\begin{aligned}\frac{\partial u}{\partial \tau} &= \frac{\sigma^2}{2}\frac{\partial^2 u}{\partial x^2}(\tau, x) + (r - \frac{\sigma^2}{2})\frac{\partial u}{\partial x}(\tau, x) - ru(\tau, x) + \\ &\quad + \int_{\mathbb{R}}\Big(u(\tau, x+y) - u(\tau, x) - (e^y - 1)\frac{\partial u}{\partial x}(\tau, x)\Big)\Pi(dy).\end{aligned} \tag{2.19}$$

Using again a change of variable we could obtain a similar equation for $V(t, S)$:

$$\frac{\partial V}{\partial t} + rS\frac{\partial V}{\partial S} + \frac{\sigma^2 S^2}{2}\frac{\partial^2 V}{\partial S^2} - rV(t, S) + \int_{\mathbb{R}}\Big(V(t, Se^y) - V(t, S) - S(e^y - 1)\frac{\partial V}{\partial S}(t, S)\Big)\Pi(dy) = 0. \tag{2.20}$$

Under the Black-Scholes model, the Lévy measure is 0 and the above equation reduces to the Black-Scholes PDE (1.4). While in the case of a finite variation Lévy process, the second order term vanishes and the derivative term under the integral can be taken out. Equation (2.20) reduces to a first order PIDE:

$$\frac{\partial V}{\partial t} + (r + \zeta)S\frac{\partial V}{\partial S} - rV + \int_{\mathbb{R}}[V(t, Se^y) - V(t, S)]\Pi(dy) = 0, \tag{2.21}$$

where $\zeta = \int(1 - e^y)\Pi(dy)$.

Chapter 3

The Black-Scholes Model

This chapter is a continuation to the article "Pricing options with discrete dividends by high order finite differences and grid stretching" by C.W. Oosterlee, C.C. Leentvaar and A. Almendral, appeared in ECCOMAS 2004, P. Neittaanmäki, et al, eds. Proc. Jyväskylä, Finland, 24-28, 2004.

3.1 Introduction

We consider option valuation under the Black-Scholes model in this chapter.

Adding a continuous dividend q to the underlying stock S, the Black-Scholes equation changes to

$$\frac{\partial V}{\partial t} + \frac{1}{2}\sigma^2 S^2 \frac{\partial^2 V}{\partial S^2} + (r-q)S\frac{\partial V}{\partial S} - rV = 0. \tag{3.1}$$

Boundary conditions arise naturally from financial arguments: The left boundary condition for a call is $V(t,0) = 0$ for all t, and a possible choice for the right-side boundary condition at a truncated boundary S_{max} (as an approximation for $S \to \infty$) is

$$V(t, S_{max}) = S_{max} e^{-r_d(T-t)} - K e^{-r(T-t)}.$$

The payoff at maturity is known and determines the final condition at $t = T$. For a European call, it reads:

$$V(T, S) = \max(S - K, 0). \tag{3.2}$$

With a simple transformation we change the equation that is backward in time into an equation forward in time and the final condition becomes initial condition. In the remaining of this chapter, we let t denote time to maturity and t_0 be the initial time. To avoid confusion, we further replace V, S by u, s respectively and rewrite the Black-Scholes equation as

$$-\frac{\partial u}{\partial t} + \frac{1}{2}\sigma^2 s^2 \frac{\partial^2 u}{\partial s^2} + (r-q)s\frac{\partial u}{\partial s} - ru = 0. \tag{3.3}$$

3.2 Grid Transformation and Discretization

We aim for an efficient and accurate procedure for obtaining the option value and the Greeks(Δ, Γ) by solving the Black-Scholes equation numerically. In order to cluster grid points in the region of interest, e.g., near the exercise price K and initial asset price s_0, an analytic grid transformation is applied. Such a transformation modifies all coefficients in the equation, but discretization can take place on an equidistant grid. Fourth order finite differences in space and time are chosen for handling this transformed equation.

3.2.1 Spatial Grid

The accuracy of a finite difference approximation depends on the existence of several derivatives in the Taylor's expansion, but in option pricing the final condition is not differentiable (or even discontinuous in the case of a digital option). Therefore, local grid refinement seems a logical choice to retain a satisfactory accuracy. It is well-known that local grid refinement near sharp corners in the domain or near singularities in an equation often improves the overall discretization accuracy drastically. By an h-refinement in the vicinity of a singularity the discretization error is locally decreased, due to the smaller h, and the global accuracy is not spoiled by the well-known *pollution effect*, as it is encountered for elliptic or parabolic equations.

The principle of local refinement is simple: Place more points in the neighborhood of the grid point where the non-differentiable condition occurs. This can be done by adaptive grid refinement for some regions, based on an error indicator, or by an *analytic coordinate transformation*, which results in an a-priori stretching of the grid. A coordinate transformation is the most elegant way in our applications as the region of interest is known beforehand. An equidistant grid discretization can be used after the analytic transformation, as only the coefficients in front of the derivatives change. We explain the principle for a general parabolic PDE with non-constant coefficients, Dirichlet boundary conditions and an initial condition:

$$\frac{\partial u}{\partial t} = \alpha(s)\frac{\partial^2 u}{\partial s^2} + \beta(s)\frac{\partial u}{\partial s} + \gamma(s)u(s,t) \tag{3.4}$$

$$u(a,t) = L(t), \quad u(b,t) = R(t), \quad u(s,0) = \phi(s). \tag{3.5}$$

Consider a coordinate transformation $y = \psi(s)$, which must be one-to-one, with inverse $s = \varphi(y) = \psi^{-1}(y)$ and let $\hat{u}(y,t) := u(s,t)$ (unknowns with "hat" live on the transformed grid). By the chain rule, the first and second derivative with respect to s of $u(s,t)$ will become:

$$\frac{\partial u}{\partial s} = \frac{\partial \hat{u}}{\partial y}\frac{dy}{ds} = \frac{\partial \hat{u}}{\partial y}\left(\frac{ds}{dy}\right)^{-1} = \frac{1}{\varphi'(y)}\frac{\partial \hat{u}}{\partial y}, \tag{3.6}$$

$$\frac{\partial^2 u}{\partial s^2} = \left(\frac{ds}{dy}\right)^{-1}\frac{\partial}{\partial y}\left(\left(\frac{ds}{dy}\right)^{-1}\frac{\partial \hat{u}}{\partial y}\right) = \frac{1}{(\varphi'(y))^2}\frac{\partial^2 \hat{u}}{\partial y^2} - \frac{\varphi''(y)}{(\varphi'(y))^3}\frac{\partial \hat{u}}{\partial y}. \tag{3.7}$$

Application of (3.6) and (3.7) to (3.4) changes the factors α, β and γ into:

$$\widehat{\alpha}(y) = \frac{\alpha(\varphi(y))}{(\varphi'(y))^2}, \quad \widehat{\beta}(y) = \frac{\beta(\varphi(y))}{\varphi'(y)} - \alpha(\varphi(y))\frac{\varphi''(y)}{(\varphi'(y))^3}, \quad \widehat{\gamma}(y) = \gamma(\varphi(y)). \tag{3.8}$$

The boundary points a and b are also transformed into $\psi(a)$ and $\psi(b)$, respectively. The equidistant grid size for the transformed equation is $h = (\psi(b) - \psi(a))/N$, assuming function ψ to be a monotonically increasing function.

The spatial transformation used for Black-Scholes equation originates from Clark and Parrot [16] and is also presented in Tavella and Randall [46]:

$$y = \psi(s) = \frac{\sinh^{-1}(\xi(s-\kappa)) - c_1}{c_2 - c_1}, \tag{3.9}$$

where $c_1 = \sinh^{-1}(\xi(a-\kappa))$ and $c_2 = \sinh^{-1}(\xi(b-\kappa))$. The grid is refined around $s = \kappa$. Usually κ is set to be K. Parameter ξ determines the rate of stretching. In the analytic function (3.9) the combination $\xi\kappa$ appears. For satisfactory accuracy, also on coarse grids, it appears advantageous to keep this quantity constant. $\xi\kappa = 15$, for example, has proven to be an appropriate choice over a variety of option pricing parameters. Figure 3.1 shows the stretching around $\kappa = 15$ for $\xi = 1$ ($\xi\kappa = 15$) and $\xi = 12$ ($\xi\kappa = 180$) and a corresponding grid. The difference in the number of points per s-interval with $\xi = 1$ and $\xi = 12$ is depicted in Figure 3.2. The number of points per interval is displayed for three grid sizes of 20, 40 and 80 points with different colors (from light to dark in Fig. 3.2). Thus, larger ξ means fewer points in the outer regions while when ξ decreases the grid approaches an equidistant one. Note that with the linear pricing rule of vanilla options, we could always normalize the strike price K to 1.

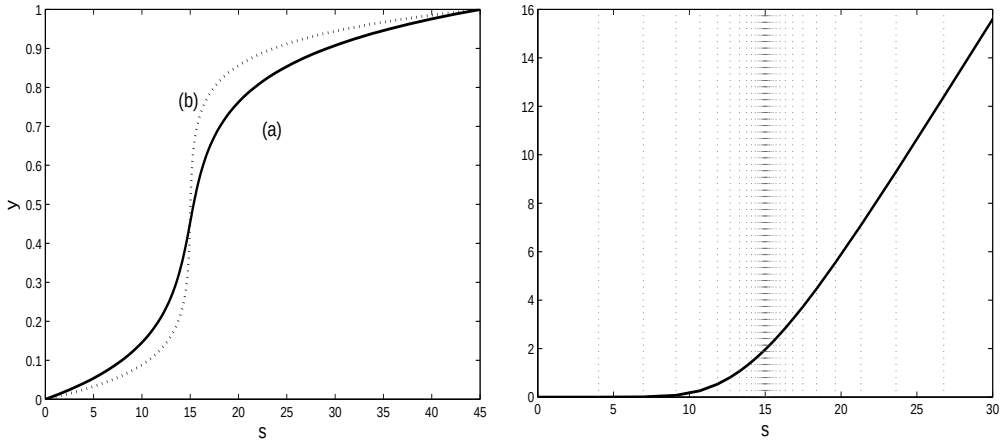

Figure 3.1: Left: Transformation function (3.9), $\kappa = 15$, (a): $\xi = 1$, (b): $\xi = 12$; Right: Example of European call option values on the stretched grid.

For transformation (3.9), the inverse and the first two derivatives are:

$$\varphi(y) = \frac{1}{\xi}\sinh(c_2 y + c_1(1-y)) + \kappa, \tag{3.10}$$

$$J(y) = \frac{c_2 - c_1}{\xi}\cosh(c_2 y + c_1(1-y)), \tag{3.11}$$

$$H(y) = \frac{(c_2 - c_1)^2}{\xi}\sinh(c_2 y + c_1(1-y)), \tag{3.12}$$

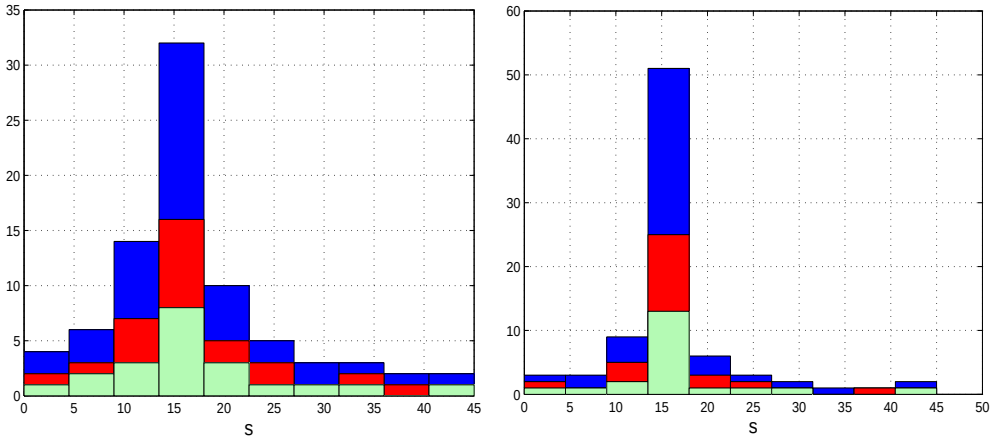

Figure 3.2: Number of grid points in an interval on the S-axis for $\xi = 1$ (left) and $\xi = 12$ (right). The total number of points is 20, 40 and 80 for the different colors from light to dark.

where $J(y)$, Jacobian, is the first derivative of $\varphi(y)$ and $H(y)$, Hessian, denotes the second derivative. Applying the transformation (3.10) to the final condition gives:

$$\hat{u}(y,T) = \max\left(\frac{1}{\xi}\sinh\left(c_2 y + c_1(1-y)\right) + \kappa - K, 0\right). \tag{3.13}$$

The sharp edge in the final condition of a European option does, thus, not disappear; the condition is not differentiable.

3.2.2 Time Grid

We aim for an implicit discretization of fourth order on an equidistant grid with time step k. A well-known family of implicit schemes with nice properties is the family of backward differentiation formulae, BDF, of which the $\mathbf{O}(k^2)$ BDF2 [24, 27] is known best. The $O(k^4)$-scheme, BDF4, is the basis for the time discretization employed. It reads

$$\left(\frac{25}{12}I - kL\right)u^{j+1} = 4u^j - 3u^{j-1} + \frac{4}{3}u^{j-2} + \frac{1}{4}u^{j-3}, \tag{3.14}$$

with k the time step, I the identity matrix, L a discrete version of operator $\mathcal{L}$ such that

$$\mathcal{L}u = \frac{1}{2}\sigma^2 s^2 \frac{\partial^2 u}{\partial s^2} + (r-q)s\frac{\partial u}{\partial s} - ru.$$

Superscript j on discrete unknown u^j represents the iteration in time.

This method needs three initialization steps. The combination of two Crank-Nicolson and one BDF3 step ($O(k^3)$) form the initialization for BDF4 here. BDF2 is known to be unconditionally stable, whereas BFD3 and BDF4 have stability regions. For our applications so far, however, the stability constraints are not problematic.

3.2.3 High Order Accuracy

A fourth order "long stencil" finite difference discretization in space based on Taylor's expansion is given by

$$\begin{aligned}\frac{\partial \hat{u}_i}{\partial t} &= \frac{1}{12h^2}\widehat{\alpha}_i\left(-\hat{u}_{i+2}+16\hat{u}_{i+1}-30\hat{u}_i+16\hat{u}_{i-1}-\hat{u}_{i-2}\right)+\\ &+\frac{1}{12h}\widehat{\beta}_i\left(-\hat{u}_{i+2}+8\hat{u}_{i+1}-8\hat{u}_{i-1}+\hat{u}_{i-2}\right)+\widehat{\gamma}_i\hat{u}_i+O(h^4),\quad 2\le i\le N-2.\end{aligned} \tag{3.15}$$

Subscript i refers to grid point $y_i = ih$ on the transformed grid. First derivatives are discretized by central differences. This is an appropriate choice as long as the equation is not convection dominating. For the fourth order approximation, interior point y_1 needs a special treatment at the left-side boundary as well as point y_{N-1} at the right-side boundary.

An approach for the first (and last) grid point is to use backward or one-sided differences, with difference scheme:

$$\frac{\partial \hat{u}_1}{\partial y} = \frac{-3\hat{u}_0-10\hat{u}_1+18\hat{u}_2-6\hat{u}_3+\hat{u}_4}{12h}+\mathbf{O}(h^4), \tag{3.16}$$

$$\frac{\partial^2 \hat{u}_1}{\partial y^2} = \frac{10\hat{u}_0-15\hat{u}_1-4\hat{u}_2+14\hat{u}_3-6\hat{u}_4+\hat{u}_5}{12h^2}+\mathbf{O}(h^4). \tag{3.17}$$

and similarly for y_{N-1}.

We also compute numerically two hedge parameters, Delta (Δ) and Gamma (Γ):

$$\Delta^s = \frac{\partial u}{\partial s},\quad \Gamma^s = \frac{\partial^2 u}{\partial s^2}\ . \tag{3.18}$$

With a fourth order accurate scheme, we find

$$\Delta_i^y = \frac{\partial \hat{u}}{\partial y} = \frac{-\hat{u}_{i+2}+8\hat{u}_{i+1}-8\hat{u}_{i-1}+\hat{u}_{i-2}}{12h}, \tag{3.19}$$

$$\Gamma_i^y = \frac{\partial^2 \hat{u}}{\partial y^2} = \frac{-\hat{u}_{i+2}+16\hat{u}_{i+1}-30\hat{u}_i+16\hat{u}_{i-1}-\hat{u}_{i-2}}{12h^2}. \tag{3.20}$$

On the s-grid the approximate derivatives read (3.6),(3.7):

$$\Delta_i^s = \left(\frac{d\varphi}{dy}\right)_i^{-1}\Delta_i^y,\quad \Gamma_i^s = \left(\frac{d\varphi}{dy}\right)_i^{-2}\Gamma_i^y-\left(\frac{d^2\varphi}{dy^2}\right)_i\left(\frac{d\varphi}{dy}\right)_i^{-3}\Delta_i^y. \tag{3.21}$$

3.3 Numerical Results with a European Option

Before we proceed to the American options, we first compute a European vanilla call to gain some insight in the properties of the numerical techniques. For the basic Black-Scholes equation closed form solutions exist. The analytic solutions serve as a reference for the numerical option prices and Greeks. Since the Greeks are often obtained by a numerical differentiation of the primary unknown u, the accuracy of these derivatives is not obvious beforehand. Theoretically, numerical differentiation reduces the accuracy

by one order. These are, however, statements on the asymptotic behavior for grid size $h \to 0$. With highly accurate discretizations, however, we expect a reasonable accuracy of the hedging parameters.

The parameters we use here are:

$$K = 15, \quad \sigma = 0.3, \quad r = 0.05, \quad q = 0.03, \quad T = 0.5. \tag{3.22}$$

We measure the error of u, Δ, Γ at initial time to the analytic solution in the infinity norm[1]. Next to this, the tables below present the error reduction factors c_∞, defined as:

$$c_\infty = \frac{\|w_{2h} - w_{ex}\|_\infty}{\|w_h - w_{ex}\|_\infty},$$

for some vector w, where w_h and w_{ex} denote the solution on mesh size h and the exact solution, respectively. We aim for accuracy with only a few grid points, therefore the grids are typically not finer than 40×40. The outer boundary s_{max} has been placed at 3 times the exercise price, according to the formula in Kangro and Nicolaides [30].

Table 3.1 presents results obtained on an *equidistant* grid for a second order scheme ($O(h^2)$ finite differences and Crank-Nicolson) and the fourth order scheme proposed. The second order scheme is the basis for many of the existing Black-Scholes based software. It is shown in Table 3.1 that second order accuracy is indeed achieved on these coarse grids, whereas the fourth order method is not performing better than second order. This is due to the lack of smoothness of the final condition. The convergence of the Greeks is satisfactorily.

Scheme	Grid	$\|u - u_{ex}\|_\infty$	c_∞	$\|\Delta - \Delta_{ex}\|_\infty$	c_∞	$\|\Gamma - \Gamma_{ex}\|_\infty$	c_∞
$\mathbf{O}(h^2 + k^2)$	10×10	1.3×10^{-1}		9.7×10^{-2}		2.1×10^{-2}	
	20×20	3.3×10^{-2}	4.0	9.6×10^{-3}	10.1	6.2×10^{-3}	3.4
	40×40	6.4×10^{-3}	5.2	1.7×10^{-3}	5.6	1.9×10^{-3}	3.3
$\mathbf{O}(h^4 + k^4)$	10×10	9.4×10^{-2}		3.0×10^{-2}		1.9×10^{-2}	
	20×20	1.6×10^{-2}	6.1	9.9×10^{-3}	3.0	3.1×10^{-3}	6.3
	40×40	4.1×10^{-3}	3.8	1.2×10^{-3}	8.2	3.6×10^{-4}	8.5

Table 3.1: Comparison of error and accuracy in u, Δ and Γ at t_0 on equidistant grids.

Table 3.2 shows results where the second and fourth order discretization are applied to the Black-Scholes equation with $\xi = 1$ ($\xi\kappa = 15$). The accuracy of the results in u, Δ and Γ is nicely improved, especially with the fourth order discretization. We do not observe the 4th order error reduction on these coarse moderately stretched grids, but the error for 20×20 points is already less than one cent (€ 0.01) with the transformation. This is a satisfactory result.

The asymptotic fourth order convergence rate is observed for larger values of ξ, i.e., with a severe stretching around the kink in the payoff. Table 3.3 confirms this for the

[1]Use of the relative error in the infinite norm, $\|(u - u_{ex})/u_{ex}\|_\infty$, was suggested. However we consider it not suitable for measuring the global accuracy, because $u_{ex} \to 0$ when $s \to 0$. An alternative can be the point-wise relative error $|(u - u_{ex})/u_{ex}|$. Some more numerical experiments show that the convergence of price and Greeks measured in this relative error at $s = K$, which is of most interest, is similar to that in terms of the absolute error in infinite norm.

Scheme	Grid	$\|u-u_{ex}\|_\infty$	c_∞	$\|\Delta-\Delta_{ex}\|_\infty$	c_∞	$\|\Gamma-\Gamma_{ex}\|_\infty$	c_∞
	10×10	6.6×10^{-2}		1.1×10^{-1}		8.5×10^{-3}	
$\mathbf{O}(h^2+k^2)$	20×20	1.8×10^{-2}	3.8	2.6×10^{-2}	4.0	3.7×10^{-3}	2.3
	40×40	4.3×10^{-3}	4.1	6.5×10^{-3}	4.0	8.5×10^{-4}	4.3
	10×10	1.1×10^{-2}		2.4×10^{-2}		6.3×10^{-3}	
$\mathbf{O}(h^4+k^4)$	20×20	1.1×10^{-3}	10.0	3.1×10^{-3}	7.6	1.3×10^{-3}	4.8
	40×40	9.4×10^{-5}	11.2	2.9×10^{-4}	10.8	9.7×10^{-5}	13.6

Table 3.2: Comparison of error and accuracy in u, Δ and Γ at t_0 *on the stretched grid*, $\xi = 1$.

option value u_h and $\xi = 12$. The convergence for Δ and Γ is also satisfactory. However, the error on the coarser grids with $\xi = 12$ is significantly larger than that obtained for $\xi = 1$ in Table 3.2. This justifies the suggested condition $\xi\kappa = 15$. The stretched grid, the solution and Greeks for $\xi = 1$ and $\xi = 12$ are displayed in Figure 3.3.

Scheme	Grid	$\|u-u_{ex}\|_\infty$	c_∞	$\|\Delta-\Delta_{ex}\|_\infty$	c_∞	$\|\Gamma-\Gamma_{ex}\|_\infty$	c_∞
	10×10	2.7×10^{-1}		1.7×10^{-1}		4.2×10^{-2}	
$\xi = 12$	20×20	1.5×10^{-2}	18.1	1.5×10^{-2}	11.5	4.2×10^{-3}	10.0
stretching	40×40	9.1×10^{-4}	16.5	1.7×10^{-3}	8.6	5.3×10^{-4}	8.0
$\mathbf{O}(h^4+k^4)$	80×80	5.7×10^{-5}	16.0	1.5×10^{-4}	11.6	4.2×10^{-5}	12.7
	160×160	3.7×10^{-6}	15.1	1.2×10^{-5}	12.4	4.2×10^{-6}	9.6

Table 3.3: Comparison of error and accuracy in u, Δ and Γ at t_0 *on the stretched grid*, $\xi = 12$.

3.4 American Options

In this section we give three different numerical examples. We consider an American call with a continuous dividend, two American puts with one discrete dividend and an American butterfly spread. In the mean time two extensions to the grid transformation scheme are introduced.

3.4.1 American Calls with a Continuous Dividend

An American style option test case has been presented in Wallner and Wystrup [48]. In the test the continuous dividend q is set such that a free boundary appears for the American call. Results were obtained on extremely fine grids with 1130 grid points in spatial and time-wise direction. Their results with finite differences were not completely convincing. The evaluation has been performed in Wallner and Wystrup [48] with the following set:

$$K = 0.9, \quad \sigma = 0.1, \quad r = 0.02, \quad q = 0.035, \quad T = 0.25. \tag{3.23}$$

We aim for satisfactorily accuracy in 40 - 80 grid points in both directions. With $K = 0.9$ we set stretching parameter $\xi = 16$ in (3.9). The outer boundary is placed at $3K$. The option value has converged on the stretched grid in fewer than 32 grid points; on the equidistant grid convergence is obtained in about 64 grid points.

We then focus on the determination of optimal exercise boundary $s_f(t)$, which is an integral part of the valuation problem. It is known that for an American call the free boundary $s_f(t)$ is a continuous, increasing function of time to maturity t. We note that, in order to get accurate $s_f(t)$ the grid is not necessarily refined at strike K, but at $max(K, \frac{r}{q}K)$ for an American call and $min(K, \frac{r}{q}K)$ for an American put at $t = T$(see Kwok [32]). Figure 3.4 compares the results obtained on a fixed stretched grid to those obtained on an equidistant grid. Although it's obvious that the stretched grid gives far better approximations than the equidistant grid (evidence can also be found in Table 3.4), we get only crude step functions for $s_f(t)$ with 40-80 grid points.

A more accurate representation of the free boundary may be achieved by applying a *time-dependent grid stretching* (hereafter called TDGS). Instead of staying with a fixed κ in transformation (3.9) for the whole duration of the option, we attempt to move κ in a way such that the grid is refined in the vicinity of the free boundary for all t. This handles especially well the case that the free boundary $s_f(t)$ runs out of the region of refinement of a *fixed grid stretching* (hereafter FGS) discussed before, which occurs constantly in the case of long maturity and high volatility. Since there's so far no tractable formula how the free boundary $s_f(t)$ evolves with respect to time to maturity t, we propose simply to extract information from the free boundary $s_f(t)$ that we get from FGS. Thus we obtain an improved free boundary $s_f^{TDGS}(t)$ by imitating the predictor-corrector scheme:

(i) *predictor*: Apply FGS with constant κ, which can be regarded as a step of pre-processing. We find $s_f^{FGS}(t)$ and the grid point $s'_f(t)$ immediately next to $s_f^{FGS}(t)$ that satisfies $u(s) > \Phi(s)$.

(ii) *corrector*: Apply TDGS with $\kappa(t)$ equal to the midpoint of $s_f^{FGS}(t)$ and $s'_f(t)$.[2]

Unlike computing the option prices, when the objective is to find accurate approximations of $s_f(t)$, we only pursue local accuracy. Thus the condition $\xi\kappa = 15$ can be relaxed in the corrector step. By choosing a large enough ξ , we can calculate $s_f^{TDGS}(t)$ on a grid that clusters almost all grid points in the region of interest. This is justified by the numerical results presented hereafter.

To assess the accuracies of schemes in computing the free boundary $s_f(t)$, we choose a 640 points grid in spatial and time-wise directions with FGS $\kappa = 0.9$ and $\xi = 16$ as our benchmark. The error measure we report is Root Mean Square(RMS) absolute error, which is defined by

$$RMS = \sqrt{\frac{1}{m}\sum_{t=\Delta t}^{m\Delta t}(s_f(t) - s_f^{REF}(t))^2}, \quad where\ m = T/\Delta t$$

[2]Assuming the error of the finite difference method is small enough and inaccuracy in determining the free boundary comes from the spatial discretization, for an American call(put) option $s_f^{FGS}(t)$ is indeed an upper(lower) bound of the true free boundary and $s'_f(t)$ is a lower(upper) bound. Choosing the midpoints is therefore a satisfactory way of compromise.

and $s_f^{REF}(t)$ is the "true" free boundary estimated from our benchmark grid.

Table 3.4 compares the RMS error in the free boundary $s_f(t)$ for different schemes, especially for 40 and 80 points TDGS with different ξ. We see that TDGS outperforms FGS. Furthermore we observe that higher ξ in TDGS yields higher accuracy in $s_f(t)$. A few more experiments show that with $\xi = 16$ the TDGS reduces the RMS error by a factor of 1.4 only, while the RMS error in $s_f(t)$ on a 40-point-grid with $\xi = 256$ is almost as small as on a 320-point-grid with $\xi = 16$. This pattern is also illustrated in Figure 3.5.

Scheme		320 points	40 points	80 points
Equidistant		3.3×10^{-3}	5.8×10^{-2}	1.7×10^{-2}
FGS		7.0×10^{-4}	6.4×10^{-3}	2.8×10^{-3}
TDGS	$\xi = 16$	-	5.2×10^{-3}	2.0×10^{-3}
	$\xi = 32$	-	2.6×10^{-3}	1.0×10^{-3}
	$\xi = 64$	-	1.3×10^{-3}	6.6×10^{-4}
	$\xi = 128$	-	1.0×10^{-3}	5.6×10^{-4}
	$\xi = 256$	-	8.9×10^{-4}	5.0×10^{-4}

Table 3.4: Comparison of RMS error in $s_f(t)$ from different schemes

We further point out that the gain of TDGS strongly depends on the volatility σ. Table 3.5 presents the RMS in $s_f(t)$ for different σ. We again adopt the parameters in (3.23) but vary σ in the range from 0.05 to 0.4. ξ is fixed at 16. TDGS is more advantageous as σ increases: the RMS errors are reduced significantly when $\sigma = 0.2 - 0.4$. Figure 3.6 shows that when $\sigma = 0.4$ the accuracy in $s_f(t)$ from an 80-point-TDGS-grid is nearly comparable to that of a 320-point-FGS-grid. Whereas when σ is as small as 0.05, the accuracy from 80 points FGS is already satisfactory and the improvement in accuracy from TDGS is negligible. This is in accordance with our expectation.

σ	80 points FGS	80 points TDGS	320 points FGS
0.05	2.3×10^{-3}	2.2×10^{-3}	5.4×10^{-4}
0.1	2.8×10^{-3}	2.0×10^{-3}	7.0×10^{-4}
0.2	5.0×10^{-3}	1.9×10^{-3}	1.3×10^{-3}
0.3	7.7×10^{-3}	2.4×10^{-3}	2.0×10^{-3}
0.4	1.1×10^{-2}	4.1×10^{-3}	2.8×10^{-3}

Table 3.5: Comparison of RMS error in $s_f(t)$ with different σ

We now investigate the Greeks. Δ and Γ obtained on equidistant grids with different resolution, from 40^2 to 320^2 points (in space and time) are presented in Figure 3.7. Δ is not accurate for 40 equidistant points, so Γ with 40 points is not displayed. Γ is not yet resolved well in 80 equidistant grid points.

Results from a fixed stretched grid are more favorable. Figure 3.8 presents Δ and Γ on FGS grids with $\xi = 16$. We also zoom in on Δ and Γ near the free boundary in the figure. In the pictures it is shown that Δ and Γ are well captured on grids with 80 grid

points. On the 40 points grid both Greeks are also well resolved except maybe at the free boundary, as the zoomed picture displays.

Improved accuracy in hedge parameters near the early exercise boundary $s_f(T)$, especially in Γ, which is discontinuous at $s_f(T)$, is automatically achieved by the application of TDGS. We report a similar pattern as shown before, that is TDGS is more powerful when σ is large. We illustrate the improvements in accuracy of Γ on an 80 points grid with $\sigma = 0.1$ and $\sigma = 0.4$ in Figure 3.9.

Another issue for accurate representation, especially of Γ near the early exercise boundary is to use one-sided and backward differences (as in (3.16),(3.17)) that do not need values across the free boundary. This way one can avoid local overshoots in Γ at the free boundary.

Figure 3.10 presents the grid convergence of the less known Greeks, Rho (u_r), Vega (u_σ), Volga ($u_{\sigma\sigma}$) and Vanna ($u_{s\sigma}$) on stretched grids varying from 40^2 to 320^2 points. In Wallner and Wystrup [48] uneconomical oscillations were observed in these Greeks for second order finite differences on coarse equidistant grids. Here, we do not observe any uneconomical oscillation in either of these Greeks, not even on grids with only 40 points. Figure 3.10 indicates that solely one peak in the Volga parameter is not accurately captured on the 40^2-grid.

3.4.2 American Puts with Discrete Dividends

We examine in this section the early exercise boundary of American puts with one discrete dividend. The case of an American call with discrete dividends is relatively easier than the put and we refer to Kwok [32].

Suppose t_d (calender time) is the time point immediately before the dividend payment. In the case of fixed dividend rate ρ, the slope of the early exercise boundary is given by

$$\lim_{t \downarrow T - t_d} s_f'(t) = rK/\rho, \tag{3.24}$$

which is independent of the volatility σ. While when the dividend is paid at a given amount D, the early exercise boundary will disappear for a period of

$$\delta t = \ln(1 + D/K)/r \tag{3.25}$$

before the ex-dividend date t_d, which is again not dependent on σ. For more details, see Appendix A or Meyer [38].

Figure 3.11 and 3.12 show the numerical results with a dividend rate $\rho = 0.02$ with FGS and TDGS. The parameters are $K = 1$, $r = 0.08$, $q = 0$, $T = 0.5$, $t_d = 0.3$, $\sigma = 0.4$. As shown in Figure 3.11, FGS only gives stairs as a representation of the free boundary when the free boundary drops to 0 at t_d and remains outside of the region of its refinement, while TDGS generates a curve with exactly the slope as given by (3.24). TDGS is certainly the better choice in this situation. We also confirm that the slope is independent of the volatility σ by the numerical results in Figure 3.12. The numerical results with a fixed dividend payment $D = 0.02$ are also coherent with the analytic results according to (3.25): $\delta t \approx 0.2475$ given the above parameters and δt remains constant with varying σ. This is demonstrated in Figure 3.13 and 3.14. In

either case the discrete dividend does not pose any specific problem and TDGS improves the accuracy in the free boundary. We further show how the s-grid evolves in time under TDGS in Figure 3.15. Every dot in the graph denotes a time-spatial grid point.

3.4.3 American Butterfly Spreads

A butterfly option has the payoff $(S-K_1)^+ + (S-K_2)^+ - 2(S-K_3)^+$, which can be thought of as a portfolio consisting of a long position in two calls with strikes K_1 and K_2 respectively and a short position in two calls with the middle strike $K_3 = (K_1+K_2)/2$.

A brief introduction to European butterfly spreads can be found in Appendix B. For an American butterfly, it is advisable to stretch the grid at all three strike prices, where the payoff is not smooth. This is achieved by defining a global Jacobian that combines the individual Jacobians for each strike price. Following Tavella and Randall [46], we use the following harmonic squared average for the combination, which yields a very smooth transformation:

$$J_k(y) = \left[(\frac{1}{\xi_k})^2 + (\varphi_k(y) - \kappa_k)^2 \right]^{\frac{1}{2}} \tag{3.26}$$

and

$$J(y) = A \left[\sum_{k=1}^{n} J_k(y)^{-2} \right]^{-\frac{1}{2}}, \tag{3.27}$$

where A is a normalization constant that must be calculated iteratively. Near each place of stretching, the global Jacobian $J(y)$ is dominated by the behavior of the local $J_k(y)$. The global transformation $s = \varphi(y)$ is then obtained by numerically integrating the global Jacobian.

The only place that needs to be taken care of is the vicinity of K_3. To attain minimal interference between the numerical solutions on grid points that lie at different sides of K_3, we choose the following lower order discretization stencils in the vicinity of K_3:

$$\frac{\partial \hat{u}_i}{\partial y} = \frac{\hat{u}_{i+1} - \hat{u}_{i-1}}{2h} + \mathbf{O}(h^2), \tag{3.28}$$

$$\frac{\partial^2 \hat{u}_i}{\partial y^2} = \frac{\hat{u}_{i+1} - 2\hat{u}_i + \hat{u}_{i-1}}{h^2} + \mathbf{O}(h^2). \tag{3.29}$$

Figure 3.16 shows the option prices with the parameters $K_1 = 0.5$, $K_2 = 1.5$, $\sigma = 0.1$, $r = 0.02$, $q = 0.015$, $T = 3$. It can also be observed that the grid has three refinement positions: K_1, K_2 and K_3. With this set of parameters we observe the occurrence of two free boundaries, one lies at left to K_3 and one at right, see Figure 3.17.

We note although it is still possible to employ TDGS to improve accuracy in the free boundaries, as also demonstrated in Figure 3.17, the combination of numerical transformation and TDGS has a serious disadvantage. If with TDGS a new numerically transformed grid is generated at each time step, it is very time-consuming compared to the analytic transformation due to the iterative solver for A and numerical integration

for the s-grid. This significantly degrades the speed of the program. However, it may not be necessary to update the grid each time step. After the predictor step, it can be decided whether or not to update the grid at a time step.

3.5 Conclusions

In this chapter we have solved the Black-Scholes equation for European and American style options with only a few grid points. Fourth order accurate space and time discretizations have been employed, using spatial grid stretching by means of an analytical coordinate transformation. With the proper choices of grid and stretching parameters, the fourth order accuracy can be achieved. Important for our applications is, however, a small discretization error with only a few grid points. This can been achieved by the techniques proposed and a moderate grid stretching. Furthermore, we have observed a satisfactory accuracy of the hedge parameters. For the European reference problem, 20 to 40 space- and time-steps are sufficient to get an accuracy of less than one cent (€ 0.01). The Greeks for an American call can be accurately resolved in 40-80 grid points. The optimal exercise boundary is also well captured in 40-80 grid points. Options on assets paying discrete dividends fit naturally in this framework and do not pose specific problems. Also more complicated strategies, like an American butterfly option, can be handled within this framework.

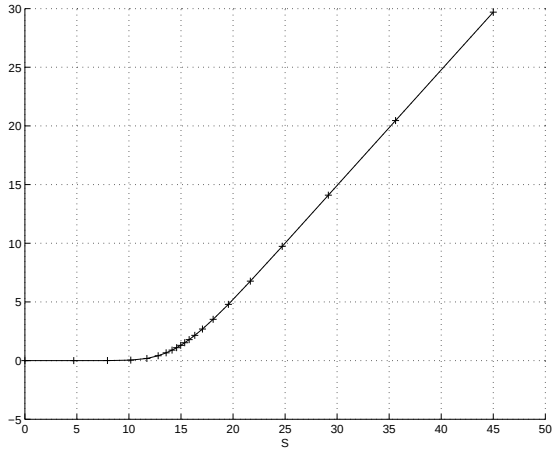

(a) u, $\xi = 1$

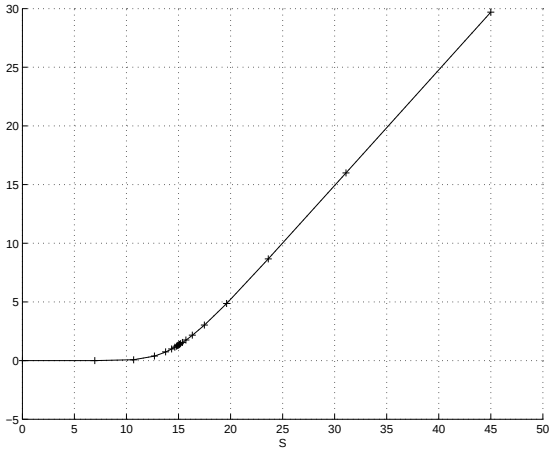

(b) u, $\xi = 12$

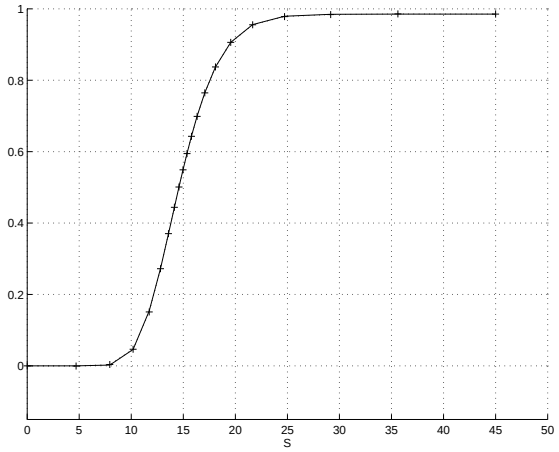

(c) Δ, $\xi = 1$

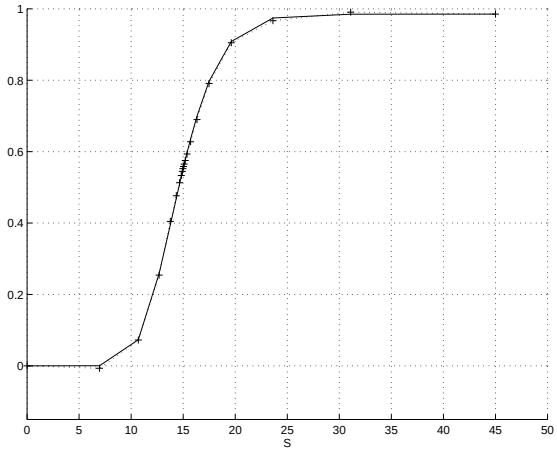

(d) Δ, $\xi = 12$

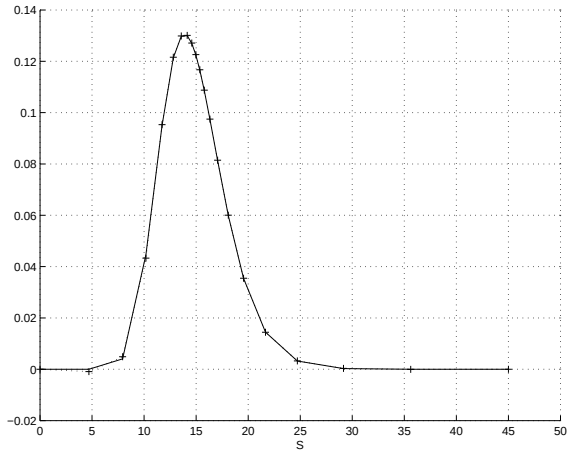

(e) Γ, $\xi = 1$

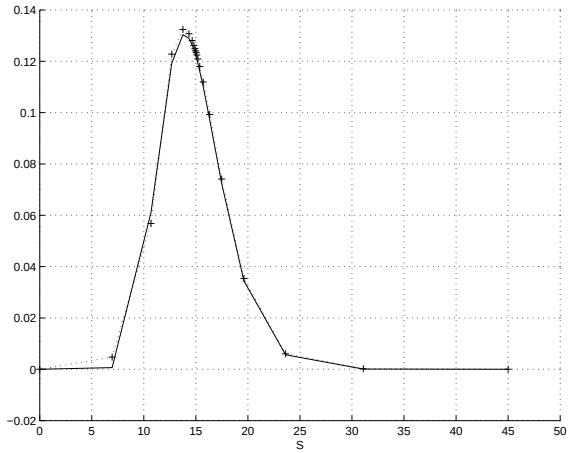

(f) Γ, $\xi = 12$

Figure 3.3: Plots of numerical option price u, Δ and Γ of a European call, $K = 15, \sigma = 0.3, d = 0.03, r = 0.05, T = 0.5$, versus the analytic solution with the 20 points stretched grids.

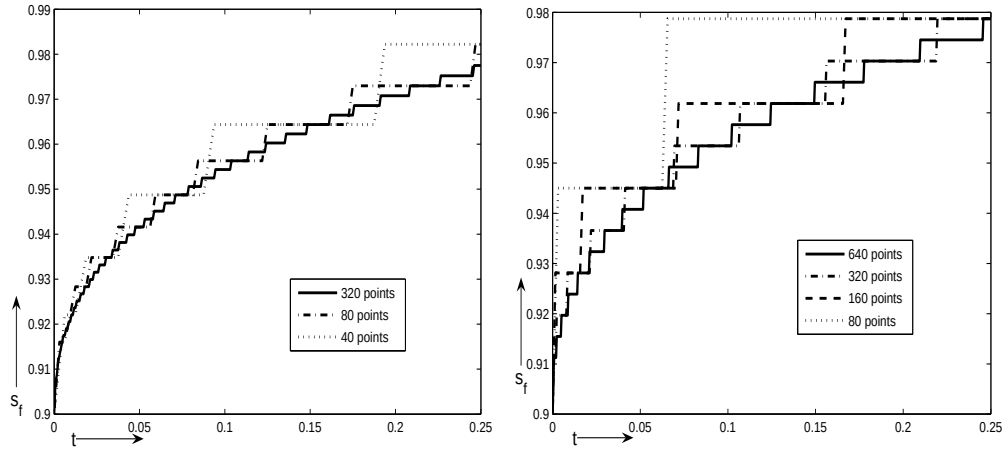

(a) stretched grid

(b) equidistant grid

Figure 3.4: The (discrete) free boundary s_f as a function of time to maturity t. Parameters are $K = 0.9, \sigma = 0.1, r = 0.02, q = 0.035, T = 0.25$.

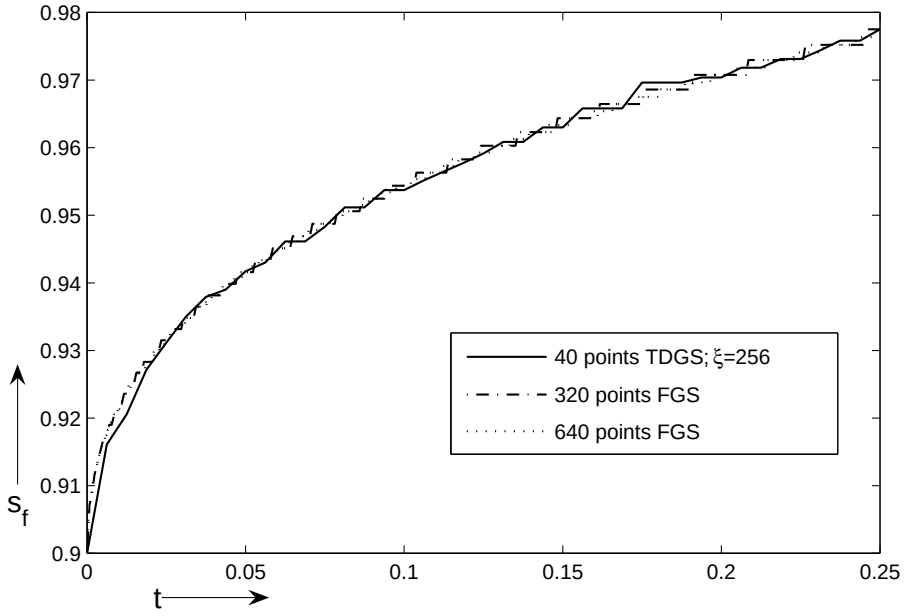

Figure 3.5: The discrete free boundary s_f as a function of time to maturity t. Parameters are $K = 0.9, \sigma = 0.1, r = 0.02, q = 0.035, T = 0.25$.

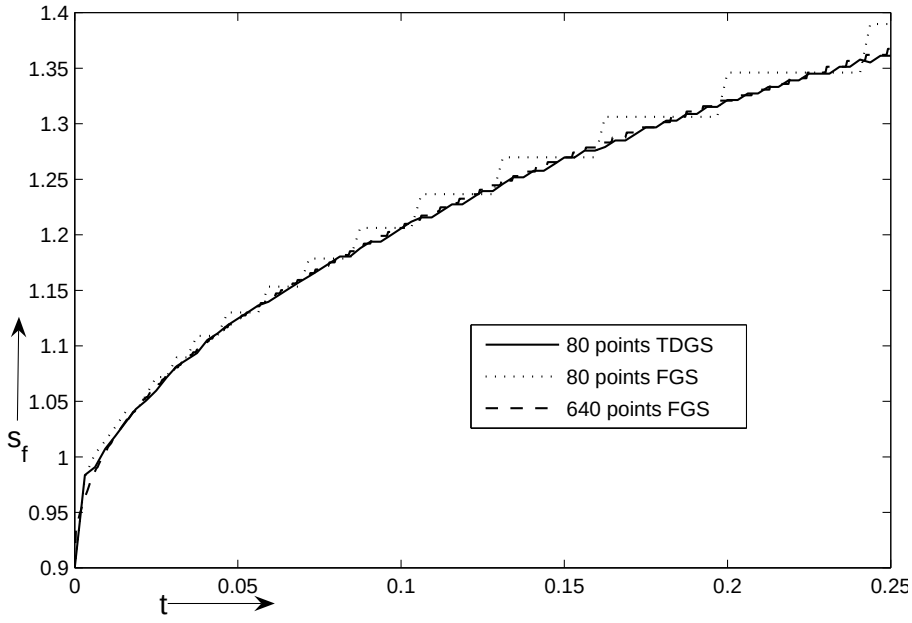

Figure 3.6: The discrete free boundary s_f as a function of time to maturity t. Parameters are $K = 0.9, \sigma = 0.4, r = 0.02, q = 0.035, T = 0.25$.

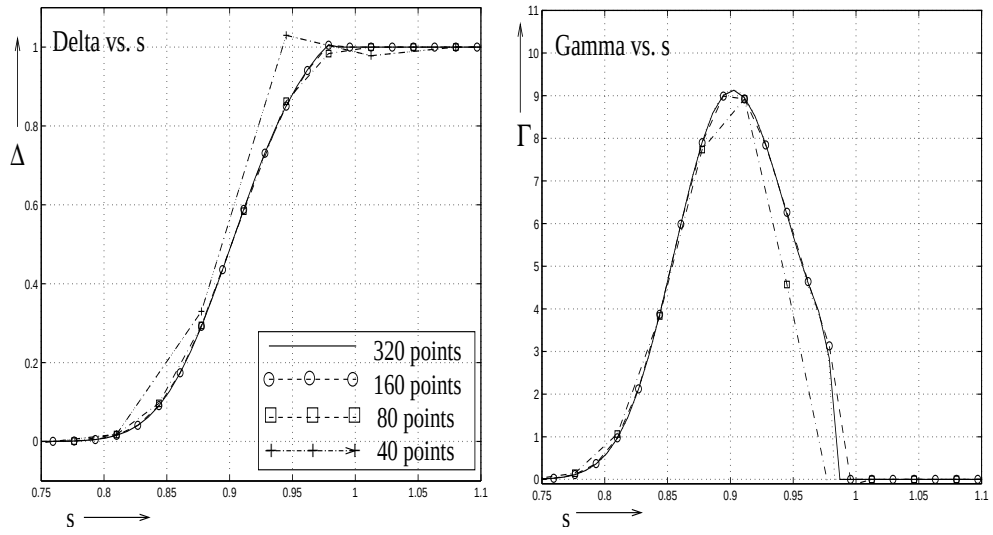

Figure 3.7: Δ and Γ for an American call on *equidistant grids* of different resolution (in the right figure the 40 points curve is omitted). Parameters are $K = 0.9, \sigma = 0.1, r = 0.02, q = 0.035, T = 0.25$.

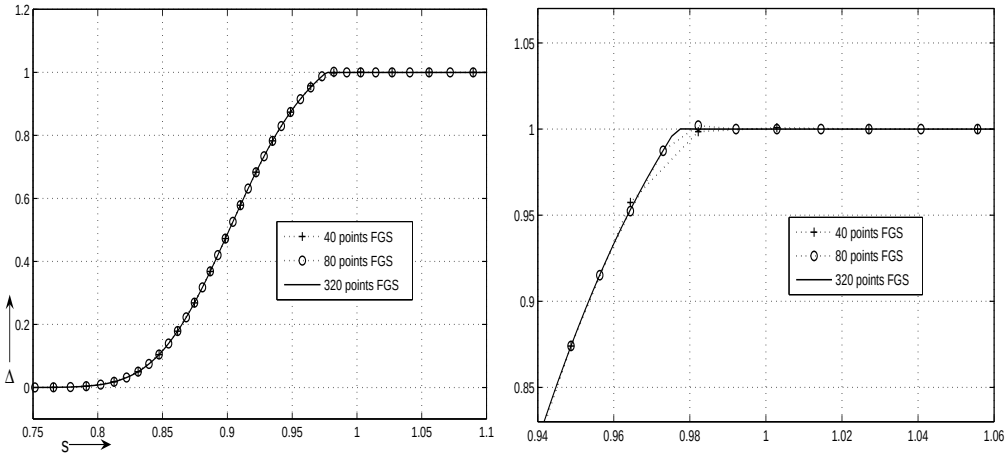

(a) Δ (b) Zoom of Δ

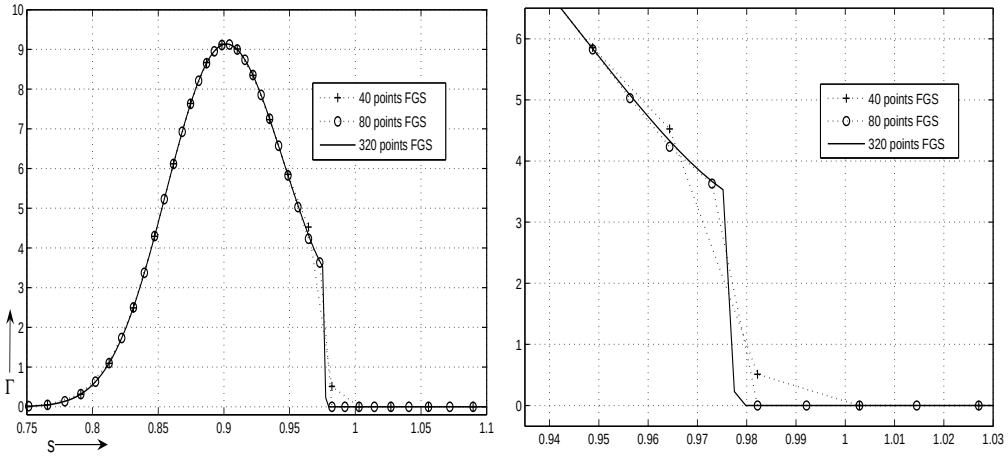

(c) Γ (d) zoom of Γ

Figure 3.8: Δ and Γ for an American call on *stretched grids* ($\xi = 16, \kappa = K$) of different resolution. Parameters are $K = 0.9, \sigma = 0.1, r = 0.02, q = 0.035, T = 0.25$.

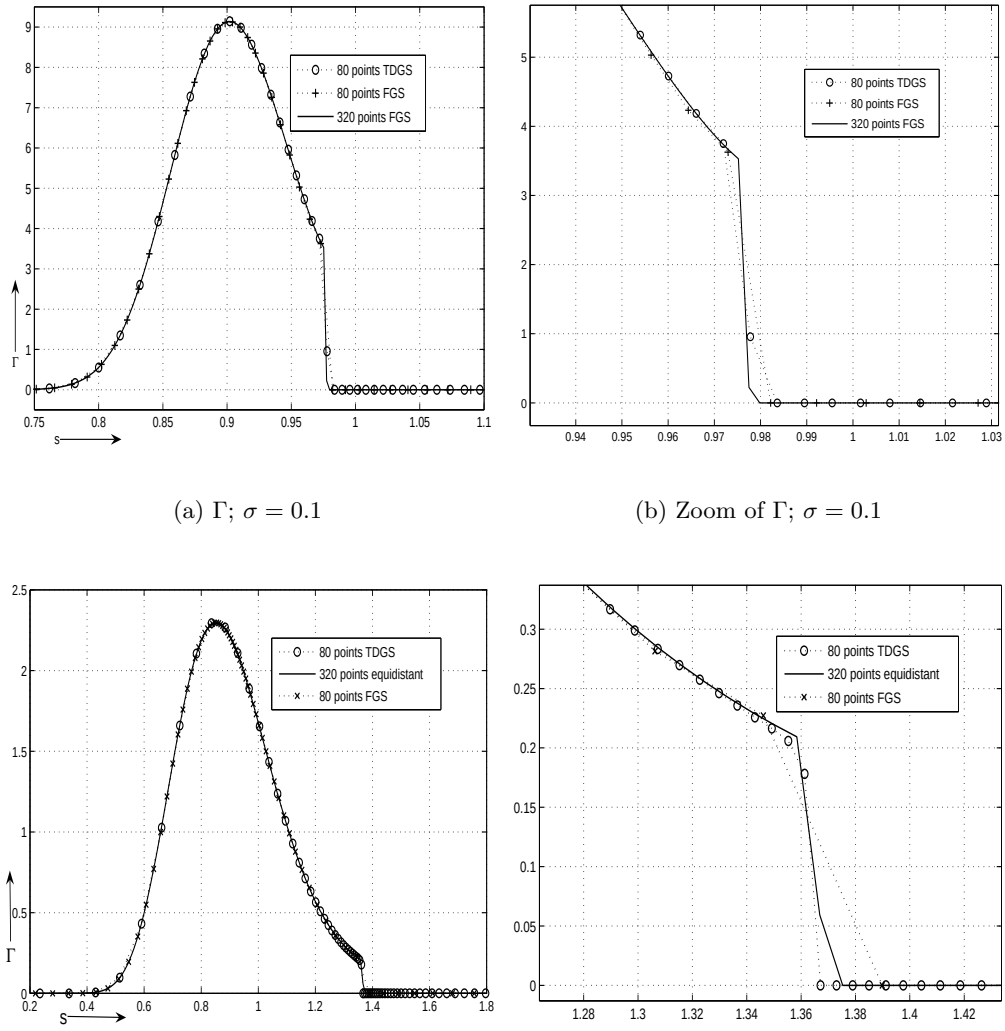

(a) Γ; $\sigma = 0.1$

(b) Zoom of Γ; $\sigma = 0.1$

(c) Γ; $\sigma = 0.4$

(d) Zoom of Γ; $\sigma = 0.4$

Figure 3.9: Comparison of Γ near the early exercise boundary for an American call obtained with FGS and TDGS for different σ. $\xi = 16$ for both schemes. Other parameters are $K = 0.9, r = 0.02, q = 0.035, T = 0.25$.

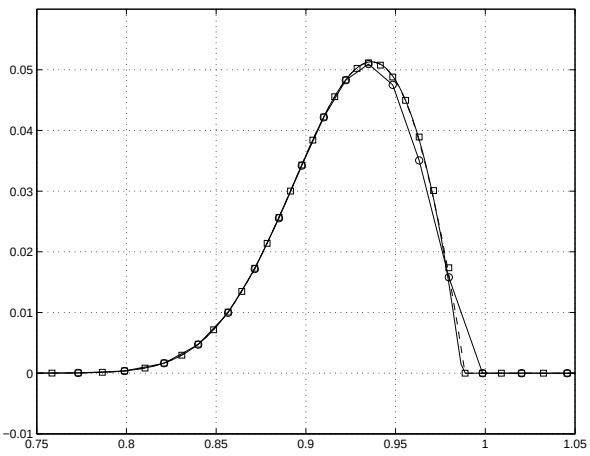

(a) Rho

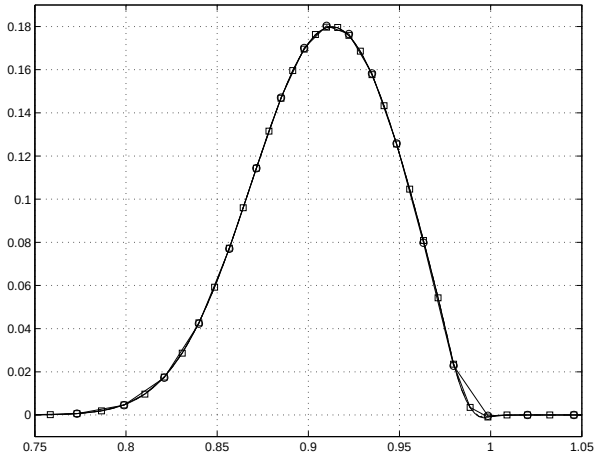

(b) Vega

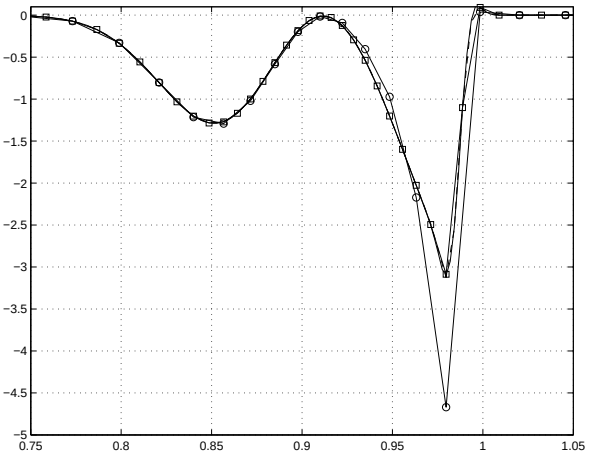

(c) Volga

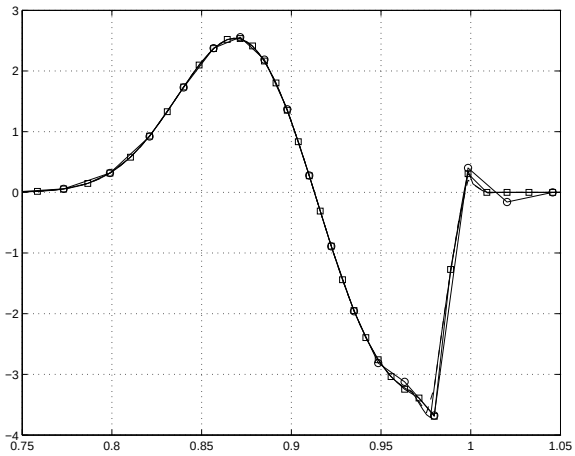

(d) Vanna

Figure 3.10: The less commonly known Greeks, Rho, Vega, Volga and Vanna, on stretched grids with different sizes. ∘ 40^2-grids, □ 80^2-grids, – – – 160^2-grids, —— 320^2-grids.

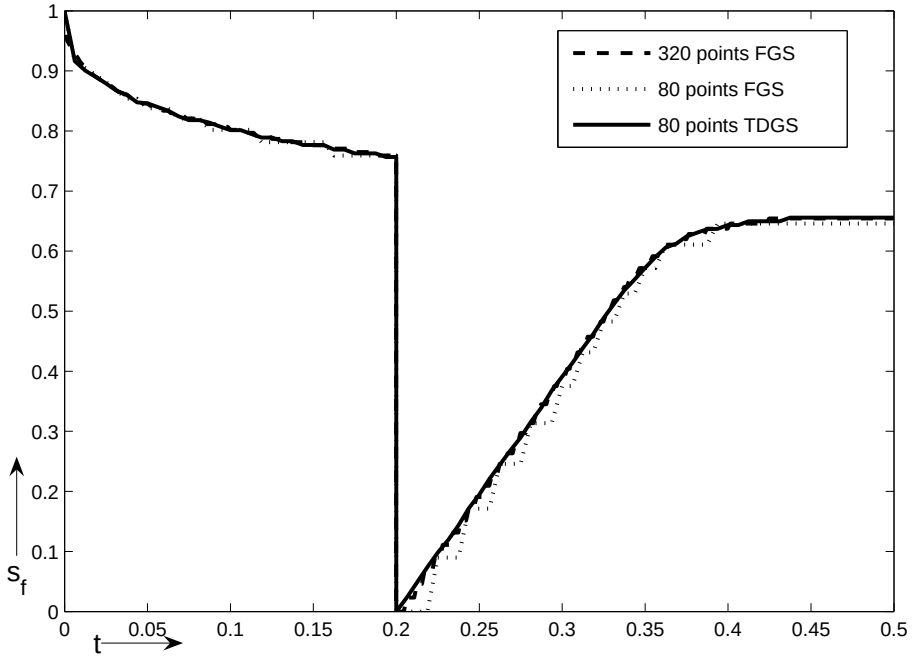

Figure 3.11: The free boundary s_f of an American put with one discrete dividend payment $\rho \cdot s$. Parameters are $K = 1, \sigma = 0.4, r = 0.08, q = 0, T = 0.5, t_d = 0.3, \rho = 0.02$.

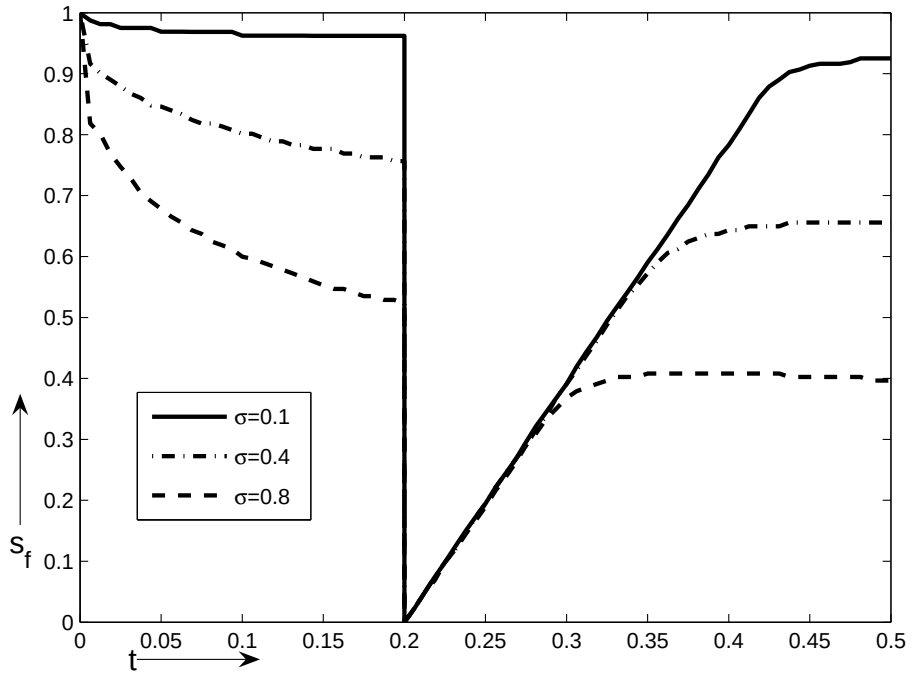

Figure 3.12: Influence of σ on the free boundary s_f of an American put with one discrete dividend payment $\rho \cdot s$, TDGS. Other parameters are $K = 1, r = 0.08, q = 0, T = 0.5, t_d = 0.3, \rho = 0.02$.

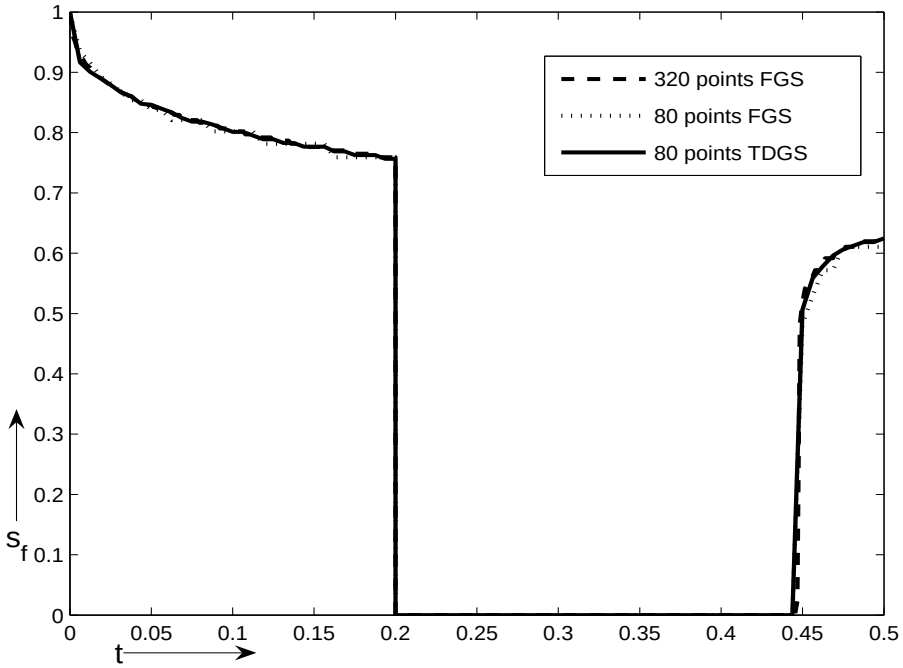

Figure 3.13: The free boundary s_f of an American put with one discrete dividend payment D. Parameters are $K = 1, \sigma = 0.4, r = 0.08, q = 0, T = 0.5, t_d = 0.3, D = 0.02$.

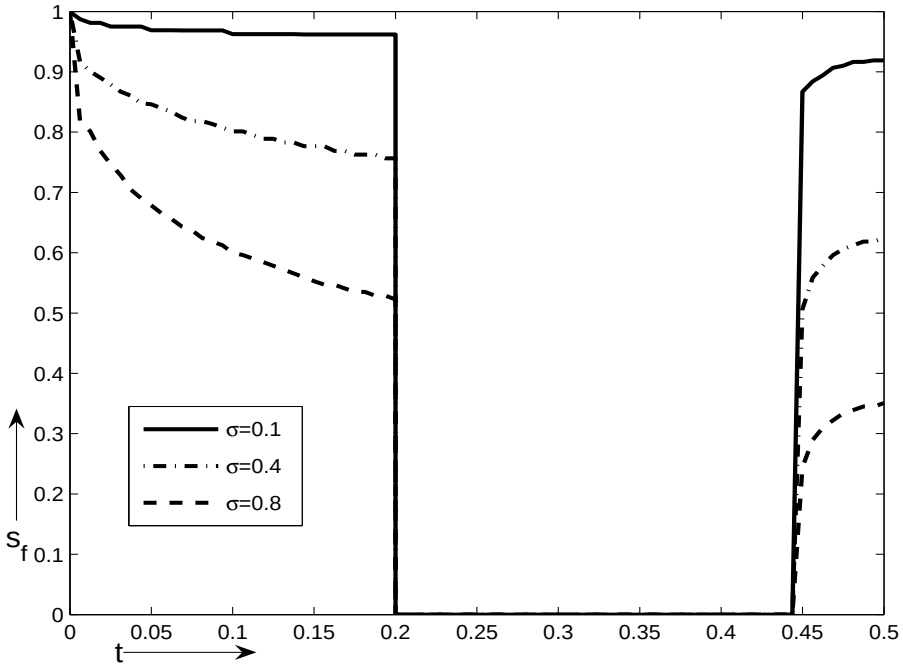

Figure 3.14: Influence of σ on the free boundary s_f of an American put with one discrete dividend payment D, TDGS. Other parameters are $K = 1, r = 0.08, q = 0, T = 0.5, t_d = 0.3, D = 0.02$.

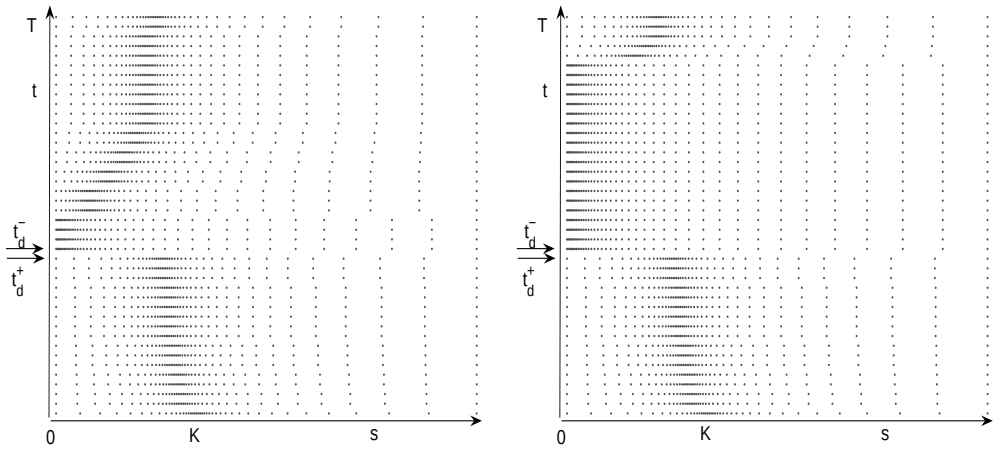

(a) fixed dividend rate (b) fixed dividend amount

Figure 3.15: The time-dependently stretched s-grid with the presence of discrete dividends. t_d^-, t_d^+ represent the times just before and after the dividend date, respectively.

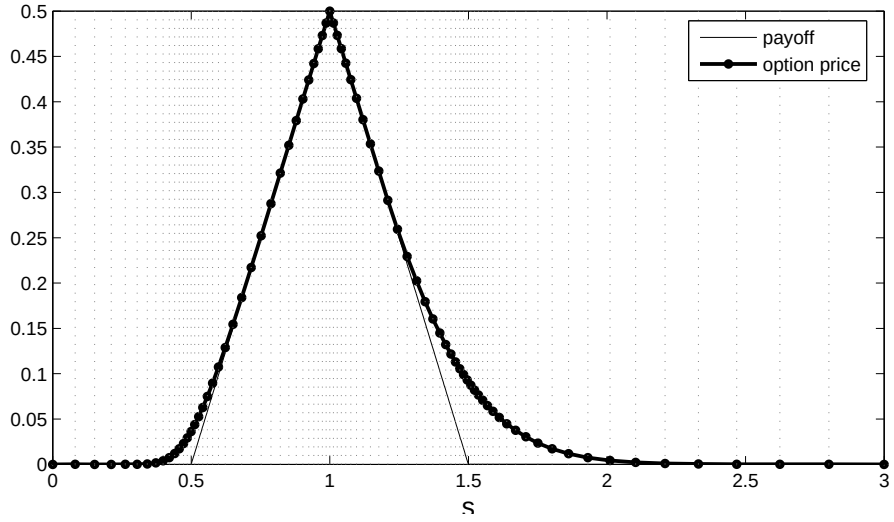

Figure 3.16: American butterfly spread price. Parameters are $K_1 = 0.5, K_2 = 1.5, \sigma = 0.1, r = 0.02, q = 0.015, T = 3$.

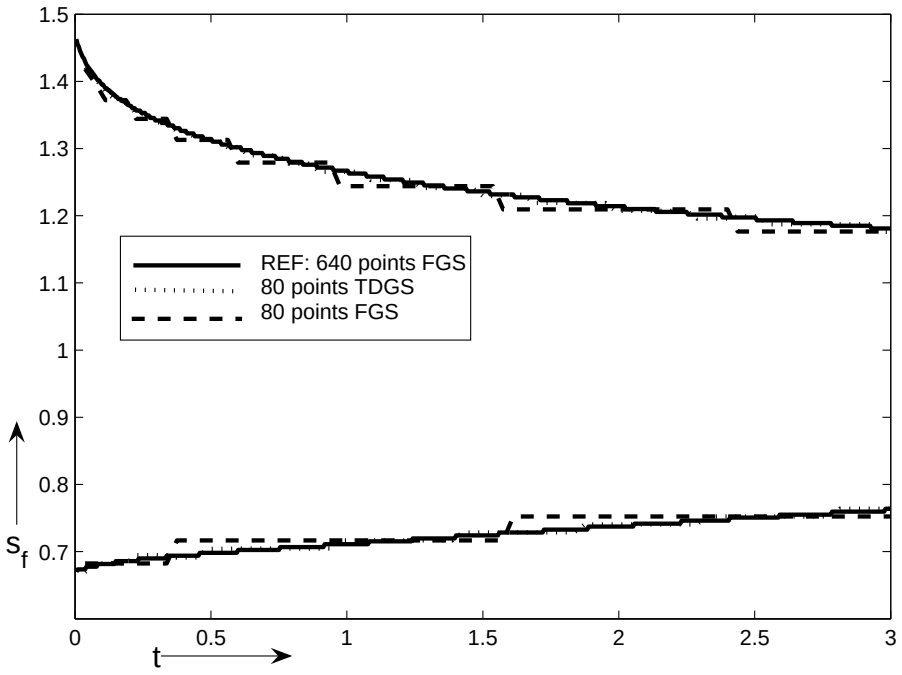

Figure 3.17: The discrete free boundaries s_f as a function of time to maturity t. The grid is stretched at three points. Parameters are $K_1 = 0.5, K_2 = 1.5, \sigma = 0.1, r = 0.02, q = 0.015, T = 3$.

Chapter 4

The Variance Gamma Model

This chapter draws heavily from the article "Highly accurate evaluation of European and American options under the variance gamma process" by A. Almendral and C.W. Oosterlee.

4.1 Introduction

This chapter develops efficient procedures for option pricing when the underlying asset is driven by the variance gamma process, which is a three parameter infinite activity, finite variation pure jump process.

Following §2.3, the log-price $x = \ln(S)$ of a European put under the Variance Gamma model satisfies the following PIDE:

$$w_t + (q - r - \zeta)w_x + rw = \int_{\mathbb{R}} [w(x + y, t) - w(x, t)]k(y)dy, \tag{4.1}$$

with initial condition

$$\Phi(x) := w(x, 0) = (K - e^x)^+, \tag{4.2}$$

where

(i) q and r are the continuous dividend yield and the interest rate respectively;

(ii) $k(y)dy = \Pi(dy)$, where $k(y)$ is called the Lévy density associated to the Variance Gamma process. We adopt here the representation as in (2.12):

$$k(y) = C\left(\frac{e^{-M|y|}}{|y|}\mathbf{1}_{\{y>0\}} + \frac{e^{-G|y|}}{|y|}\mathbf{1}_{\{y<0\}}\right). \tag{4.3}$$

(iii) For ζ we have the following expression

$$\zeta = \int_{\mathbb{R}} (1 - e^y)k(y)dy = C\ln[(1 + 1/G)(1 - 1/M)].^1 \tag{4.4}$$

[1] In order for ζ to be defined, $M > 1$ must be satisfied.

(iv) t denotes the time to expiration, that is, the equation is written forward in time.

Let $\alpha = q - r - \zeta$, the convection term in (4.1) may be removed by using the following change of variables

$$u(x,t) = w(x + \alpha t, t). \tag{4.5}$$

Then $u_t = w_t + \alpha w_x$ and u satisfies the equation

$$u_t + ru = \int_{\mathbb{R}} [u(x+y,t) - u(x,t)]k(y)dy, \tag{4.6}$$

which does not contain the convection term.

Let $\mathcal{I}(u)$ denote the integral term on the right-hand side of (4.6). The price of an American put option is then given as the solution to the following Linear Complementarity Problem in terms of u:

$$\begin{cases} u_t + ru \geq \mathcal{I}(u) & \text{in } (0,T] \times \mathbb{R}, \\ u \geq \Phi(x + \alpha t) & \text{in } [0,T] \times \mathbb{R}, \\ (u_t + ru - \mathcal{I}(u))\,(u - \Phi(x + \alpha t)) = 0 & \text{in } (0,T] \times \mathbb{R}, \\ u(x,0) = \Phi(x). \end{cases} \tag{4.7}$$

4.2 Grid Transformation and Discretization

4.2.1 Spatial Grid

Similar to the idea in §3.2.1, we employ a convenient non-linear change of variable to smooth the payoff function at the point of singularity $\ln K$. We again call it FGS. Grid stretching with the spatial transformation function

$$\varphi(a) = \kappa + sgn(a - \kappa)|a - \kappa|^m, \quad m \geq 1. \tag{4.8}$$

to an equidistant grid in the variable a is applied. The new grid is refined at κ and the parameter m controls the degree of stretching. The transformed payoff function $\Phi(\varphi(a))$ is displayed in Figure 4.1 for different degrees of stretching.

The advantage of this transformation is two-fold: on one hand, more points are situated around the kink of the payoff, and on the other hand, fewer points describe the growth at infinity. As a consequence, the integral is now localized on a smaller interval.

4.2.2 Evaluation of the Integral Term

The convolution form of the integral term of (4.1), though convenient for FFT purposes, does not easily allow the change of variables from the grid stretching. An alternative form is preferable, so we first change to the variable $z = x + y$, and then we set $z = \varphi(b)$,

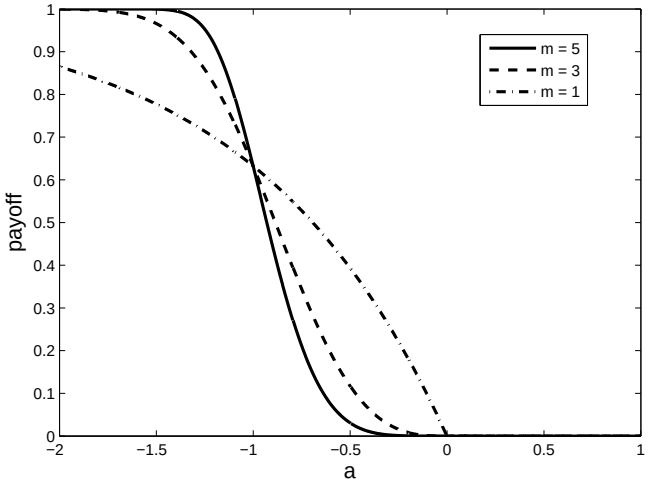

Figure 4.1: Transformed payoff function for different values of m.

$x = \varphi(a)$. Thus, the a-grid will be the computational grid and the b-grid is used for the integration. This yields

$$\begin{aligned}\int_{-\infty}^{+\infty} &[u(x+y) - u(x)]k(y)dy \\ &= \int_{-\infty}^{+\infty} [u(z) - u(x)]k(z-x)dz \\ &= \int_{-\infty}^{+\infty} [v(b) - v(a)]k(\varphi(b) - \varphi(a))\varphi'(b)db \\ &= \int_{-\infty}^{a} G_a(b)k_1(a,b)db + \int_{a}^{\infty} G_a(b)k_1(a,b)db \end{aligned} \tag{4.9}$$

where $v(b) := u(\varphi(b))$ and we have introduced the functions

$$G_a(b) := \frac{v(b) - v(a)}{b - a} \quad \text{and} \quad k_1(a,b) := k(\varphi(b) - \varphi(a))\varphi'(b)(b-a). \tag{4.10}$$

For ease of notation, we sometimes omit the variable t in $v(a,t)$. The reason for the splitting at $b = a$ is because the integrand changes sign at this point. Note that each term in (4.9) has now the form of a *Volterra integral operator* of the first kind, as the variable a appears in the integration limit. The corresponding integral equations have been studied numerically, see for example Brunner and van der Houwen [11]. For the discretization of these operators we use a direct quadrature method, see §4.2.4 below.

4.2.3 Truncating the integral

In this section we determine a bound for the error when truncating the integrals (4.9) to a finite domain. To this goal, we restrict the domain of variable x to a bounded interval of the form $\Omega_\rho^* = [B_0^* + \rho,\ B_1^* - \rho]$, for a certain $\rho > 0$, and consider the error

$$\varepsilon(x) := \int_{\mathbb{R}/\Omega^*} (u(z) - u(x))k(z-x)dz, \tag{4.11}$$

where Ω^* is the enlarged interval $\Omega^* := [B_0^*,\ B_1^*]$. Our objective is to show that this error may be bounded uniformly for x belonging to Ω_ρ^*.

We carry out the reasoning for the positive semiaxis, (for the negative semiaxis the reasoning goes similarly), using the fact that the VG European option in log-prices satisfies the inequality

$$|u(z) - u(x)| \leq Ke^{-rt}|z - x|, \quad \forall z, x \in \mathbb{R}. \tag{4.12}$$

This is a consequence of the mean value theorem combined with the fact that the absolute value of the Delta is bounded everywhere by Ke^{-rt}; see Appendix C for a proof. This yields

$$\begin{aligned}
|\varepsilon(x)| &= C \int_{B_1^*}^{+\infty} \frac{|u(z) - u(x)|}{|z - x|} e^{-M(z-x)} dz \\
&\leq Ke^{-rt} C e^{Mx} \int_{B_1^*}^{\infty} e^{-Mz} dz \\
&= Ke^{-rt} C \frac{e^{M(x - B_1^*)}}{M} \\
&\leq Ke^{-rt} C \frac{e^{-M\rho}}{M}, \quad \forall x \in \Omega_\rho^*.
\end{aligned}$$

That is, we find a bound that holds uniformly in the x variable, and that depends on the parameter ρ: the larger ρ, the better the approximation by truncation. However, a better estimate may be obtained in the new variable a that exploits the fact that the transformed integrand is more 'localized'. Define the interval $\Omega_\delta := [B_0 + \delta, B_1 - \delta]$, for a given number $\delta > 0$ and write $x = \varphi(a)$ and $B_1^* = \varphi(B_1)$. By the mean value theorem, one obtains the following lower bound

$$B_1^* - x = \varphi(B_1) - \varphi(a) \geq \varphi(B_1) - \varphi(B_1 - \delta) \geq \varphi'(B_1 - \delta)\delta. \tag{4.13}$$

provided φ' is increasing (which is the case for φ given in (4.8)). We arrive at the error estimate

$$|\varepsilon(a)| \leq Ke^{-rt} C \frac{e^{-M\varphi'(B_1 - \delta)\delta}}{M}. \tag{4.14}$$

Observe that this upper bound decreases rapidly for values of m between 2 and 4, which we typically use in our computations.

We may now summarize the criterion. In order to determine the truncation interval Ω_δ, one decides first a certain margin δ and a tolerance ϵ. Thereafter, one computes the integration limits B_0 and B_1 by solving the following two inequalities

$$\begin{cases} Ke^{-rt} C \frac{e^{-M\varphi'(B_1 - \delta)\delta}}{M} < \epsilon, \\ \\ Ke^{-rt} C \frac{e^{-G\varphi'(B_0 + \delta)\delta}}{G} < \epsilon. \end{cases} \tag{4.15}$$

4.2.4 Simpson's Rule

We dedicate this part to explain how Simpson's rule may be applied to obtain a highly accurate evaluation of the integrals in (4.9). Let $f(x)$ be a smooth function in the

interval $[x_0, x_{2n}]$ and define the nodes $x_i = x_0 + ih$, for $i = 0, 1, \ldots, 2n$ and mesh width $h = (x_{2n} - x_0)/2n$. The compound Simpson's rule states that

$$\begin{aligned}\int_{x_0}^{x_{2n}} f(x)dx =& \frac{h}{3}[f_0 + 4(f_1 + f_3 + \cdots + f_{2n-1}) \\ &+ 2(f_2 + f_4 + \cdots + f_{2n-2}) + f_{2n}] + \varepsilon_n \end{aligned} \tag{4.16}$$

and the error term $\varepsilon_n = O(h^4)$, provided $f \in C^4[x_0, x_{2n}]$; see for example Davis and Rabinowitz [18]. Note that an odd number of points $x_0, \ldots, x_{2n}$ is necessary to use this rule.

We now apply Simpson's rule to (4.9). Let $a_{\min} := B_0$ and $a_{\max} := B_1$ according to the notation in §4.2.3. Next, consider a uniform grid for the variable a as follows: let N be some integer and define the nodes $a_i = a_{\min} + (i-2)h$ $(i = 1, \ldots, N+2)$ where $h = (a_{\max} - a_{\min})/N$. In particular this means $a_1 = a_{\min} - h$ and $a_2 = a_{\min}$. Once we know the sampling points a_i, we approximate the truncated integrals

$$J_i = \int_{a_{\min}}^{a_i} \frac{v(b) - v(a_i)}{b - a_i} k_1(a_i, b)db. \tag{4.17}$$

We use for the integration variable b the same grid spacing, namely, $b_j = a_{\min} + jh$ $(j = 0, \ldots)$. Hence, to be able to apply Simpson's rule, one has to choose even values of the index i in (4.17), since the number of nodes b_j in $[a_{\min}, a_i]$ has to be odd. In other words, we cannot approximate (4.17) for i odd. A remedy to fill these gaps is to apply Simpson's rule on the integrals

$$J_i = \int_{a_{\min}-h}^{a_i} \frac{v(b) - v(a_i)}{b - a_i} k_1(a_i, b)db, \quad i = 1, 3, \ldots. \tag{4.18}$$

Another strategy could be to use the composite Simpson's 3/8 rule for i odd, see Brunner and van der Houwen [11]. Special care should be taken at the end point $b = a_i$, for each i, since there is an avoidable singularity. To deal with this situation numerically, a second-order one-sided discretization has been chosen.

The integrand is a continuous function in the closed interval $[a_{\min}, a_i]$ for the family of functions (4.8). In the open interval $(a_{\min}, a_i)$ this integrand belongs to C^{m-1}, where m is the degree of smoothness of the change of variable φ. This is a crucial observation that confirms the accurate results in the next section.

An important remark is that the method outlined here is computationally intensive since it requires $O(N^2)$ operations to compute all the integrals J_i. It is the subject of current research to increase the speed of evaluation of these integral transforms, for which methods like Multilevel integration in Brandt and Venner [10] or Hierarchical matrices in Hackbusch [26] may be suitable.

4.2.5 A Deviation: Fast Convolution by Fast Fourier Transform(FFT)

The fast Fourier transform (FFT) is a discrete Fourier transform algorithm which reduces the number of computations needed for N points from $O(N^2)$ to $O(N \log_2 N)$. Unfortunately it is only applicable to matrices resulting from equidistant grid discretization.

We nevertheless include a brief introduction on the computation of convolutions by the FFT since in the sequel we assess our grid stretching approach on the basis of solutions obtained by FFT method[2]. For more general information on the FFT algorithms, see van Loan [47].

The Discrete Fourier Transform(DFT) is defined as

$$F_n = \mathcal{F}_k[\{f_k\}_{k=0}^{N-1}](n) = \sum_{k=0}^{N-1} f_k e^{-2\pi i n k/N}, \quad n = 0, 1, ..., N.$$

Suppose $\{h_k\}$ and $\{g_k\}$ are two sequences with period N. The convolution of these two sequences is another sequence $\{f_k\}$ defined by

$$f_k = \sum_{n=0}^{N-1} g_n h_{k-n}. \tag{4.19}$$

Let F, G and H denote the DFT of the sequence f, g and h respectively, we then have

$$F_n = G_n \cdot H_n.$$

The sequence f_k then can be recovered by Inverse Discrete Fourier Transform(IDFT)

$$f_k = \mathcal{F}_n^{-1}[\{F_n\}_{n=0}^{N-1}](k) = \frac{1}{N} \sum_{n=0}^{N-1} F_n e^{2\pi i k n/N}, \quad k = 0, 1, ..., N$$

The computation of f_0,...,f_{N-1} in (4.19) corresponds to the product of an N-by-N *circular matrix* and an N-dimensional vector. For example, suppose N=3,

$$\begin{bmatrix} f_0 \\ f_1 \\ f_2 \end{bmatrix} = \begin{bmatrix} h_0 & h_2 & h_1 \\ h_1 & h_0 & h_2 \\ h_2 & h_1 & h_0 \end{bmatrix} \begin{bmatrix} g_0 \\ g_1 \\ g_2 \end{bmatrix}. \tag{4.20}$$

Another matrix/vector product that can be similarly handled is with a *Toeplitz* matrix, which is constant along its diagonals. The matrix representation of the integral term to be evaluated in (4.6),

$$\int_{\mathbb{R}} u(x+y)k(y)dy,$$

falls into this type.

Assuming the components of matrices are indexed from zero, it is possible to construct a M-by-M circular matrix C, with $M \geq 2N-1$, from a N-by-N Toeplitz matrix T such that $T = C(0 : N-1, 0 : N-1)$. For example, the following Toeplitz matrix

$$\begin{bmatrix} u_1 & u_0 & u_{-1} \\ u_2 & u_1 & u_0 \\ u_3 & u_2 & u_1 \end{bmatrix} \tag{4.21}$$

[2]This FFT method is not the one from either Carr and Madan [13] or Lewis [33], FFT is only used for fast evaluation of the convolution. For more details on the procedures, we refer to Almendral and Oosterlee [3].

can be embedded in the circular matrix[3]

$$\begin{bmatrix} u_1 & u_0 & u_{-1} & u_3 & u_2 \\ u_2 & u_1 & u_0 & u_{-1} & u_3 \\ u_3 & u_2 & u_1 & u_0 & u_{-1} \\ u_{-1} & u_3 & u_2 & u_1 & u_0 \\ u_0 & u_{-1} & u_3 & u_2 & u_1 \end{bmatrix}. \tag{4.22}$$

Let $\tilde{k} = \begin{bmatrix} k \\ 0 \end{bmatrix}$ and $\tilde{J} = C\tilde{k}$, then the product J of Toeplitz matrix T and vector k is given by

$$J = Tk = C(0:N-1, 0:N-1)k = C(0:N-1,:)\tilde{k} = \tilde{J}(0:N-1).$$

In this way fast evaluation of $C\tilde{k}$ permits fast evaluation of Tk.

4.2.6 Time Integration

We evaluate the explicit BDF2 method to solve (4.6) and (4.7), with initial condition (4.2). It is observed that the equation is not stiff and therefore an explicit method is appropriate.

First, we rewrite (4.6) in terms of the new function $v(a,t) = u(\varphi(a), t)$:

$$v_t + rv = \int_{-\infty}^{\infty} \frac{v(b,t) - v(a,t)}{b-a} k_1(a,b)db. \tag{4.23}$$

We denote now by $\mathcal{J}(v)$ the integral operator on the right hand side of (4.23). The approximation of the integral operator described in §4.2.4 is denoted by $J(v)$. Let $v_i^j \approx v(a_i, t^j)$ be an approximation to the solution at times $t^j = jk$ $(j = 0, \ldots, L)$ and spatial points a_i. By v^j we mean the vector of spatial unknowns (v_i^j). Likewise, a stands for the vector (a_i).

For the European option under the VG process, the explicit BDF2 method reads

$$\frac{3}{2}v^j - 2v^{j-1} + \frac{1}{2}v^{j-2} + krv^j = kJ(\bar{v}^j), \quad \text{where} \quad \bar{v}^j = 2v^{j-1} - v^{j-2}. \tag{4.24}$$

This leads to a simple iteration of the form $v^j = \hat{J}(v^{j-1}, v^{j-2})$. The first input to this iteration is the payoff v^0 and the second, v^1, is the result of one explicit Euler iteration. Note that the update $\bar{v}^j$ is obtained by linear extrapolation.

The discrete solution to the American case is also straightforward, since for BDF2 the corresponding discrete LCP may be written as

$$\begin{cases} v^j \geq \hat{J}(v^{j-1}, v^{j-2}) \\ v^j \geq \Phi(\varphi(a) + \alpha t^j) \\ \langle v^j - \hat{J}(v^{j-1}, v^{j-2}), v^j - \Phi(\varphi(a) + \alpha t^j) \rangle = 0 \\ v^0 = \Phi(\varphi(a)). \end{cases} \tag{4.25}$$

[3]Usually M is chosen to be power of 2 to fully exploit the computational efficiency of the FFT algorithm.

Here $\langle \cdot, \cdot \rangle$ is the standard inner product in $\mathbb{R}^d$. The solution of this problem is simply $v^j = \max(\hat{J}(v^{j-1}, v^{j-2}), \Phi(\varphi(a) + \alpha t^j))$.

4.3 Numerical Results with a European Option

We proceed with some numerical experiments on a European put option, with the following parameters:

$$K = 1, \quad r = 0.1, \quad q = 0, \quad C = 1, \quad G = 5, \quad M = 5, \quad T = 0.5. \tag{4.26}$$

The effect of the stretching factor is tested by comparing $m = 1, 2, 3$. We take $B_0 = -3$, $B_1 = 3$, irrespective of the transform parameter m. κ is set to be $\ln K = 0$. We compute the solution $u(z, T)$ of equation (4.6) by solving (4.23) on the stretched grid, and later apply the shift (4.5) to recover the solution, i.e., $w(x, T) = u(x - \alpha T, T)$. An interpolation is needed at this stage as the grid points $x_i - \alpha T$ will not necessarily coincide with the points on the x-grid. Cubic splines are used to interpolate to this new grid.

We take the solution computed with FFT on a uniform grid with 96,000 spatial points and 9,600 time steps as our benchmark and denote it as w^{REF}. The errors and the empirical rates of convergence in the infinity norm ($\|w^N - w^{REF}\|_\infty$, denoted as l_∞-error later on), are presented in Table 4.1. A stretched grid is able to significantly improve the option price estimates. The reduction in errors grows rapidly as the grid size increases. With moderate stretching ($m = 2$), we confirm BDF2's second order convergence in time. With a more severe stretching ($m = 3$) a higher order convergence is observed. The combination of grid stretching ($m = 3$), explicit BDF2 and Simpson's rule is taken to evaluate an American option.

Grid		m=1		m=2		m=3	
N	L	l_∞-error	rate	l_∞-error	rate	l_∞-error	rate
20	10	1.7×10^{-2}	-	6.1×10^{-3}	-	7.6×10^{-3}	-
40	20	5.7×10^{-2}	3.0	1.7×10^{-3}	3.6	1.8×10^{-3}	4.3
80	40	1.9×10^{-3}	3.0	4.9×10^{-4}	3.5	2.1×10^{-4}	8.3
160	80	5.7×10^{-4}	3.3	1.0×10^{-4}	4.9	1.7×10^{-5}	12

Table 4.1: l_∞-error for the European put option with different stretching parameter m. Rate is the rate of changes in error.

In the Black-Scholes model the Greeks are important to determine a hedging portfolio, while in the presence of jumps their importance is not so clear since in general a perfect hedge does not exist. Our computation of Greeks is solely to illustrate the scope of the stretching method. The Delta(Δ) in Figure 4.2 is computed by numerically differentiating the solution w.

We note the Delta(Δ) for European option can also be obtained by differentiating equation (4.1) with respect to x. Let $\bar{w} := w_x$, we arrive at the same equation in terms of $\bar{w}$,

$$\bar{w}_t + (q - r - \omega)\bar{w}_x + r\bar{w} = \int_{\mathbb{R}} (\bar{w}(x + y, t) - \bar{w}(x, t))k(y)dy,$$

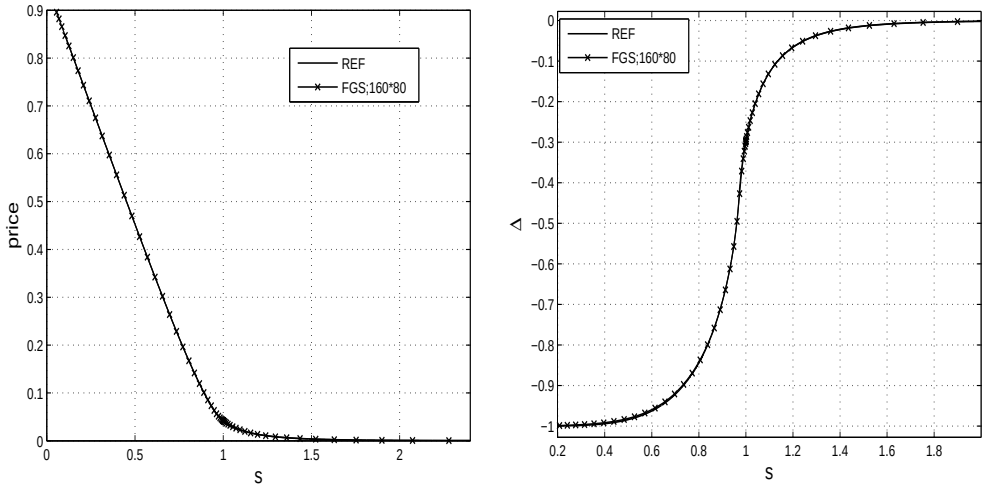

(a) option price

(b) Delta(Δ)

Figure 4.2: European put option price and option Delta on a FGS grid.

but with initial condition $\bar{w}(x,0) = -\exp(x)\mathbf{1}_{\{x<\ln K\}}$.

4.4 The American Put Option

We evaluate an American put option on a fixed stretched grid with $m = 3$ and $\kappa = \ln K$. The parameters are the same as in (4.26) except that we adopt a longer maturity: $T = 3$. This is to better illustrate the behavior of the optimal exercise boundary.

In Table 4.2 we display the pointwise convergence rates of the at-the-money option price with strike $K = 1$. With the chosen parameters we encounter the case where the "smooth pasting" condition is not valid (see e.g. Alili and Kyprianou [1], Almendral [2], Almendral and Oosterlee [3]). We illustrate this phenomenon in Figure 4.3. This accounts for loss in accuracy with respect to the European counterpart. As we may observe, the rate of convergence is still high, but the algorithm is more demanding on the time restriction. Therefore, we choose $N = L$ instead of $N = 2L$ for the European case. w^{REF} is computed by FFT method on a 96000×32000 grid. We see in Table 4.2 with 160×160 points, we already get result accurate to 5^{th} decimal point.

N	L	w	absolute error	rate
20	20	0.10203	6.8×10^{-3}	-
40	40	0.095558	2.8×10^{-4}	24.3
80	80	0.095308	3.3×10^{-5}	8.5
160	160	0.095279	3.8×10^{-6}	8.7
REF		0.0952751	-	-

Table 4.2: Pricing error and convergence for at-the-money American option by FGS, $m = 3$. Absolute error is defined by $|w^N - w^{REF}|$. Rate is the rate of changes in error.

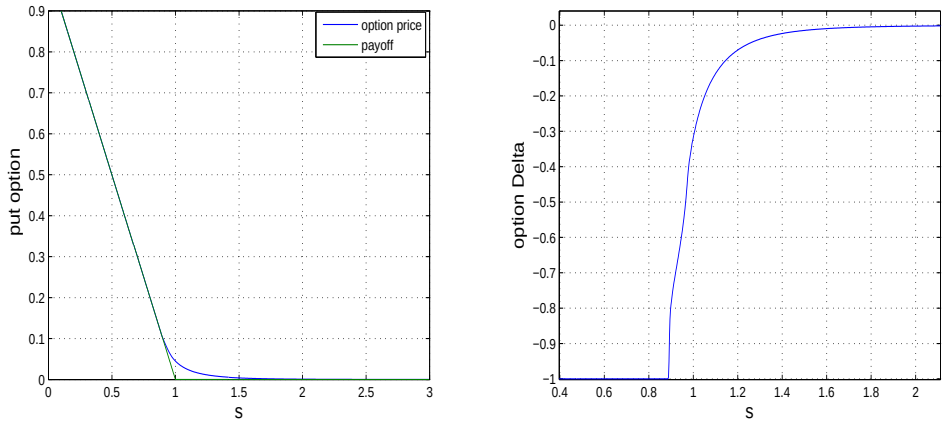

(a) option price

(b) Delta(Δ)

Figure 4.3: American put option price and option Delta. The non-smooth fit situation is clearly observed in the Delta.

In addition, we compare the FGS method to the FFT method in terms of accuracy and speed. The results are reported in Figure 4.4, plotted on a log-log scale. Computation time is measured on a desktop with Pentium(R) 4 CPU 2.4GHz and 512MB of RAM. Implementations of both methods are in MATLAB. $N = 3L$ for FFT and $N = 2L$ for FGS are chosen with care in order to tune the methods to produce best possible results. The FGS is at least as competitive as the FFT method and it prevails when requirement in accuracy is high. It is certainly not surprising: the equidistant grid FFT based method is known to be only first order accurate and demands a large number of points to achieve high accuracy.

A straightforward fixed grid stretching however does not determine the free boundary accurately on coarse grids, given the sparsity of the mesh points around the free boundary. The time dependent grid stretching(TDGS) as introduced in §3.4 is readily at disposal to resolve this problem. We show in Table 4.3 the improvement in accuracy of free boundary in terms of both RMS and l_∞-error with TDGS based on FGS with the same grid size. Both errors are roughly reduced by a factor of 4 consistently. In Figure 4.5, we compare the free boundaries obtained by FGS and TDGS on a 320×160 grid to the benchmark. The free boundaries from TDGS and the benchmark are not easily distinguishable while the improvement from FGS to TDGS is conspicuous. We also observe that the free boundary does not start at the strike K. This pattern differs from the situation under Black-Scholes model and is also exhibited in Matache, Nitsche and Schwab [39].

We further point out that the preprocessing step need not necessarily to be FGS. FFT on a coarse grid is an ideal alternative for preprocessing since it is fast (but not accurate), e.g., the FFT approach on a 1000×160 grid costs roughly only one-tenth of the time of FGS on a 160×160 grid(roughly 1.5:15 in seconds). Figure 4.6 illustrates the free boundary obtained by TDGS based on a FFT preprocessing: TDGS on a 320×160 grid

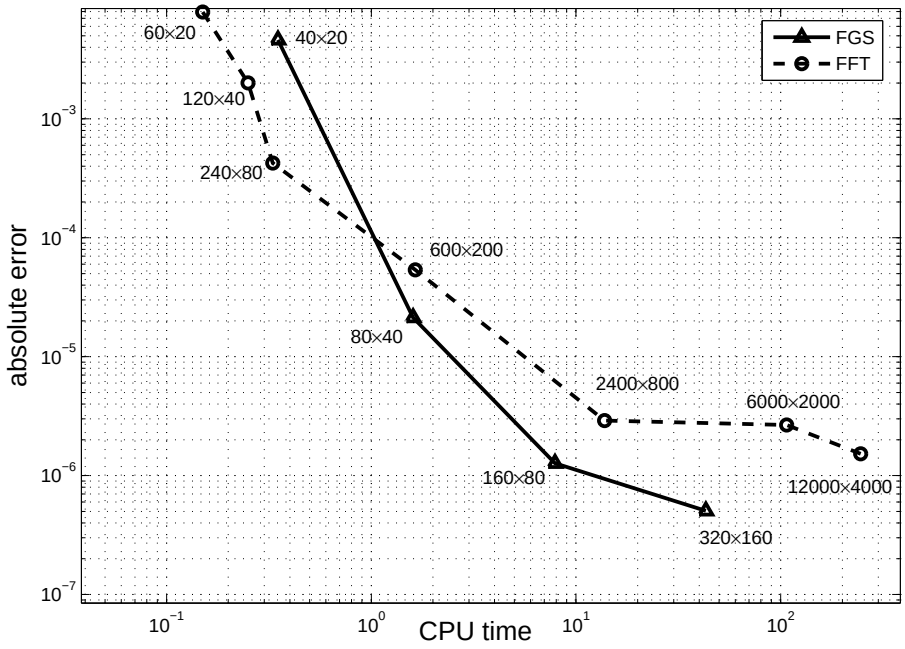

Figure 4.4: Speed-accuracy tradeoff for at-the-money American put: comparison between FGS and FFT. Numbers next to the points indicate the grid size. FFT are computed on grids with $N = 3L$. Results of FGS are based on those grids with $N = 2L$. Parameters are $K = 1, r = 0.1, q = 0, C = 1, G = 5, M = 5, T = 3$.

and FFT on a 1000×160 grid.

4.5 Conclusions and Perspectives

We have in this chapter computed European and American vanilla option prices assuming the underlying process is of VG type. It has been shown that working with a refined grid around the kink $x = \ln K$ of the payoff function helps to increase the accuracy of the numerical integration, and in particular a higher precision of the option price can be reached with only a few points on the grid. The optimal exercise boundary for American style options is well captured by a time-dependent grid stretching. The method is easy to implement and is at least as competitive as the FFT method. It can be extended to

Grid		RMS		l_∞-error	
N	L	FGS	TDGS	FGS	TDGS
80	80	1.5×10^{-2}	6.3×10^{-3}	3.2×10^{-2}	1.5×10^{-2}
160	160	9.1×10^{-3}	2.0×10^{-3}	2.1×10^{-2}	5.3×10^{-3}
320	160	5.6×10^{-3}	1.2×10^{-3}	1.1×10^{-2}	2.9×10^{-3}
320	320	5.2×10^{-3}	8.5×10^{-4}	1.1×10^{-2}	2.8×10^{-3}

Table 4.3: Reduction in RMS and l_∞-error in the free boundary by TDGS based on FGS with the same grid size, $m = 3$.

other types of infinite activity, finite variation Lévy processes.

A possible improvement in the future is to expedite the computation of convolution on a nonuniform grid by using methods like Multilevel integration.

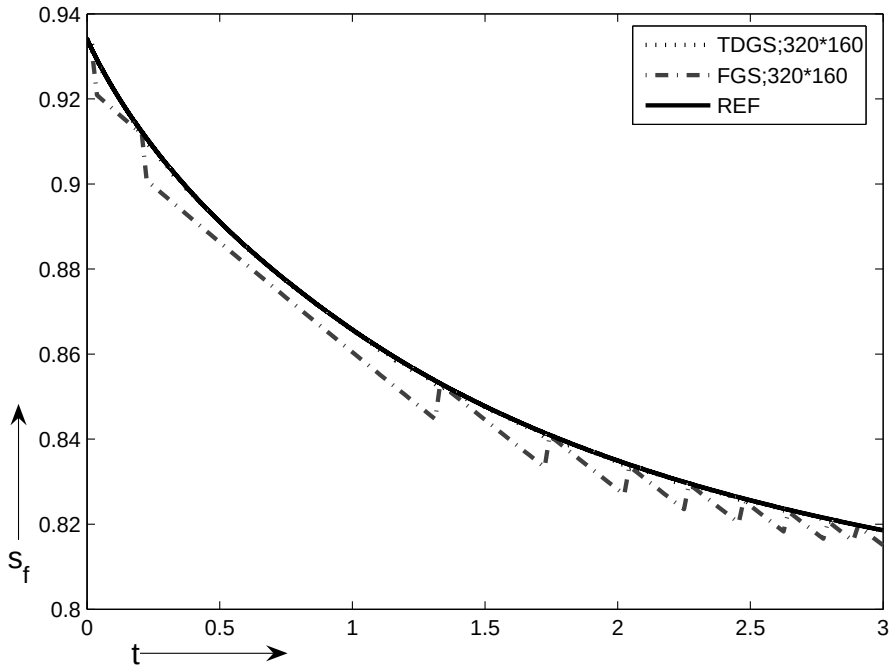

Figure 4.5: The discrete free boundary s_f as a function of time to maturity t, $m = 3$. Parameters are $K = 1, r = 0.1, q = 0, C = 1, G = 5, M = 5, T = 3$.

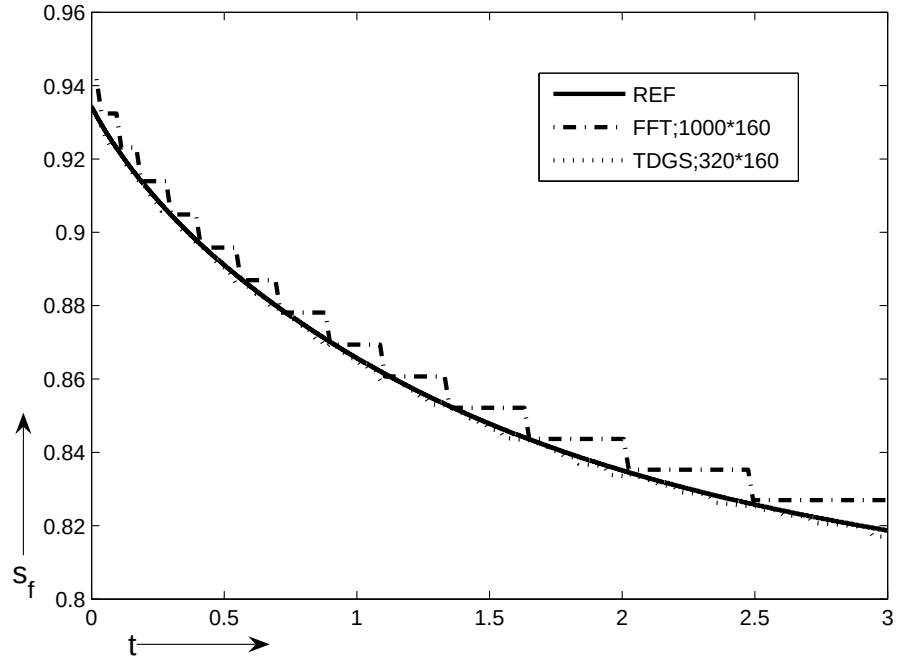

Figure 4.6: The discrete free boundary s_f as a function of time to maturity t, $m = 3$, FFT as a preprocessing tool. Parameters are $K = 1, r = 0.1, q = 0, C = 1, G = 5, M = 5, T = 3$.

Appendix A

Early Exercise Boundary of American Puts with Discrete Dividends

Consider an American put under the Black-Scholes framework with strike K and maturity T. Suppose a dividend is to be paid at time t_d and t_d^-, t_d^+ represent the times just before and after the dividend date, respectively. Note this t_d and t below are both calendar time.

It is well known that in $[0, t_d^-)$ and $[t_d^+, T)$ the value $V(t, S)$ of the option is the solution of the Black-Scholes equation. Therefore from the time t_d^+ to T, the optimal exercise boundary behaves the same as that of a non-dividend paying American put.

We now investigate the period before the dividend payment. From the no-arbitrage principle, the underlying asset will decline by the same amount as the dividend right after the payment, i.e.,

$$S_{t_d^+} = f(S_{t_d^-}), \tag{A.1}$$

where

$$f(S) = (1 - \rho)S \tag{A.2}$$

if the dividend is paid at a fixed rate ρ, or

$$f(S) = S - D \tag{A.3}$$

if the dividend is paid at a fixed amount D. Moreover the option price must be continuous across the instant of discrete dividend, i.e.,

$$V(t_d^-, S_{t_d^-}) = V(t_d^+, S_{t_d^+}). \tag{A.4}$$

The holder of a deep in-the-money American put would tend to defer exercise until t_d^+ in order to benefit from the decline in the price of the underlying asset after dividend payment. Hence we have

$$S_f(t_d^-) = 0.$$

Let us first consider the case of fixed dividend rate ρ. Assume we have a portfolio consisting a stock S and a put option P. At some time prior to the dividend date $t = t_d - \delta t$, if we exercise the option the interest income from t to t_d is $Ke^{r\delta t}$; if we hold the option and exercise immediately after the dividend payment, say t_d^+, the gain is $K + \rho S_{t_d^-}$, which is stochastic up to time t. The free boundary $S_f(t)$ is determined by matching profit in the risk neutral world in the two strategies. With fixed dividend rate ρ this leads to

$$K[e^{r\delta t} - 1] = \rho E^Q[S_{t_d^-}|\mathcal{F}_t] = \rho e^{r\delta t} S_f(t) = \rho e^{r\delta t}[S_f(t) - S_f(t_d^-)]. \tag{A.5}$$

Taking the limit $\delta t \to 0$ we get

$$\lim_{t \to t_d^-} s_f'(t) = -rK/\rho. \tag{A.6}$$

In the case of fixed dividend amount D, the gain of the above portfolio changes to $K+D$ if we exercise the option at t_d^+. Early exercise is not optimal if

$$Ke^{r\delta t} < K + D, \tag{A.7}$$

which indicates that the early exercise boundary will disappear for a period of

$$\delta t = \ln(1 + D/K)/r \tag{A.8}$$

before the ex-dividend date t_d.

Appendix B

European Butterfly spreads

A European butterfly option can be thought of as a portfolio consisting of a long position in two calls with strikes K_1 and K_2 respectively and a short position in two calls with the middle strike $K_3 = (K_1 + K_2)/2$. All the options should have the same maturity date. The payoff of such a portfolio is $(S - K_1)^+ + (S - K_2)^+ - 2(S - K_3)^+$. Note the use of European puts at the same strike prices results in exactly the same payoff.

A European style butterfly is appropriate when the investor thinks large moves in the price of the underlying asset are unlikely. It usually has a middle strike K_3 around the spot price s_0 of the underlying asset and it pays off when the price of the underlying asset stays close to s_0.

The price of a European butterfly is simply the sum of the prices of the four options in the portfolio. The typical payoff and price of a European butterfly are shown in Figure B.1. We see it is a limited risk, limited return strategy.

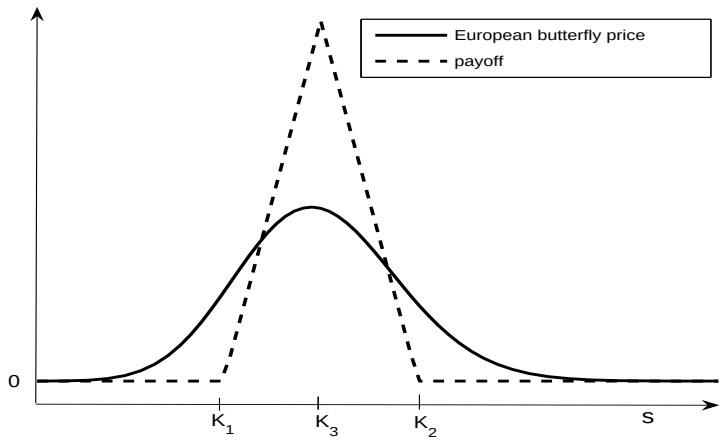

Figure B.1: Payoff and price of a European butterfly spread.

Appendix C

Upper Bound for the option Delta in log-prices

In §4.2.3 we made use of the following estimate for the Delta in log-prices

$$\left|\frac{\partial w}{\partial x}(x,t)\right| < Ke^{-rt}. \tag{C.1}$$

In fact, we used this bound on the shifted function u instead, but we derive it here for the original function w. Recall that we are working with a put option under the VG process.

The solution w of (4.1) has the following stochastic interpretation

$$w(x,t) = e^{-rt}E^Q[\psi(x + L_{T-t})], \tag{C.2}$$

where $\{L_t\}_{t\geq 0}$ is the Lévy process defined in terms of the VG process $\{X_t\}_{t\geq 0}$, i.e., $L_t := -\alpha t + X_t$. The expectation has been taken with respect to a risk-neutral measure. Denoting by $q(y)$ the probability density function of the variable L_{T-t}, we may write

$$\begin{aligned} w(x,t) &= e^{-rt}\int_{-\infty}^{\ln K - x}(K - e^{x+y})q(y)dy & \text{(C.3)}\\ &= e^{-rt}\{K\int_{-\infty}^{\ln K - x} q(y)dy - e^x\int_{-\infty}^{\ln K - x} e^y q(y)dy\}. & \text{(C.4)} \end{aligned}$$

Differentiation with respect to x on the last equality gives

$$\frac{\partial w}{\partial x} = e^{-rt}\{-Kq(\ln K - x) - [e^x\int_{-\infty}^{\ln K - x} e^y q(y)dy - e^x e^{\ln K - x}q(\ln K - x)]\}. \tag{C.5}$$

This expression simplifies into

$$\frac{\partial w}{\partial x} = -e^{-rt}e^x\int_{-\infty}^{\ln K - x} e^y q(y)dy. \tag{C.6}$$

The upper bound (C.1) now follows since e^y is less than Ke^{-x} on the interval $(-\infty, \ln K - x)$, and the integral of $q(y)$ over this interval is less than one.

Bibliography

[1] L. Alili and A.E. Kyrianou, *Some remarks on first passage of Lévy processes, the American put and pasting principles*, To appear in The Annals of Applied Probability, 2005.

[2] A. Almendral, *Numerical valuation of American options under the CGMY process,* Exotic Option Pricing under Advanced Lévy Models, A.E. Kyprianou and Wilmott,eds., 2004.

[3] A. Almendral and C.W. Oosterlee, *On American options under the variance gamma process,* 2005, submitted for publication.

[4] A. Almendral and C.W. Oosterlee, *Highly accurate evaluation of European and American options under the variance gamma process,* 2005, submitted for publication.

[5] D. Applebaum, *Lévy process and stochastic calculus,* Cambridge University Press, 2004.

[6] L. Bachelier, *Théorie de la spéculation,* Annales de l'Ecole Normale Supérieure, 3, Paris: Gauthier-Villars, 1900

[7] G. Bakshi, C. Cao, Z. Chen, *Empirical Performance of Alternative Option Pricing Models,* J. OF FINANCE, 52(5): 2003-2049, 1997.

[8] O. Barndorff-Nielsen, *Processes of Normal Inverse Gaussian type,* Finance and Stochastics, 2: 41-68, 1998.

[9] F. Black and M. Scholes, *The pricing of options and corporate liabilities,* Journal of Political Economy, 81: 637-654, 1973.

[10] A. Brandt and C.H. Venner, *Multilevel evaluation of integral transforms with asymptotically smooth kernels,* SIAM Journal of Scientific Computing, 19(2): 468-492, 1998.

[11] H. Brunner and P. J. van der Houwen, *The numerical solutions of Volterra equations,* vol. 3 of CWI Monograph, North-Holland Publishing Co., Amsterdam, 1986.

[12] P. Carr, H. Geman, D. Madan and M. Yor, *The fine structure of asset returns: an empirical investigation,* Journal of Business 75(2): 305-332, 2002.

[13] P. Carr and D. Madan, *Option valuation using the fast Fourier transform,* Journal of Computational Finance, 2(4): 61-73, 1999.

[14] P. Carr and L. Wu, *The Finite Moment Log Stable Process and Option Pricing,* Journal of Finance, 58(2): 753-778, 2002.

[15] R. Cont, P. Tankov, *Financial modelling with jump processes,* Chapman & Hall / CRC Press, 2003.

[16] N. Clarke, K. Parrot, *Multigrid for American option pricing with stochastic volatility,* Appl. math. finance, 6: 177-179, 1999.

[17] C.W. Cryer, *The solution of a quadratic programming problem using systematic overrelaxation,* SIAM J. Control, 9: 385-392, 1971.

[18] P.J. Davis and P. Rabinowitz, *Methods of numerical integration,* Computer Science and Applied Mathematics, Academic Press Inc., Orlando, FL, 2nd ed., 1984.

[19] F. Delbaen and W. Schachermayer, *A General Version of the Fundamental Theorem of Asset Pricing,* Mathematische Annalen, 300: 463-520, 1994.

[20] F. Delbaen and W. Schachermayer, *The Fundamental Theorem of Asset Pricing for Unbounded Stochastic Processes,* Mathematische Annalen, 312: 215-250, 1998.

[21] E. Eberlein and U. Keller, *Hyperbolic distributions in finance,* Bernoulli, 1(3): 281-299, 1995.

[22] E. Eberlein, U. Keller and K. Prause, *New insights into smile, mispricing and value at risk: The hyperbolic model,* Journal of Business 71(3): 371406, 1998.

[23] E.F. Fama, *The behavior of stock market prices,* Journal of Business, 34: 420-429, 1965.

[24] C.W. Gear, *Numerical initial value problems for ordinary differential equations.* Prentice-Hall, Englewood Cliffs NJ, 1971.

[25] H.U. Gerber and E.S.W. Shiu, *Option pricing by Esscher transforms,* Transactions of the Society of Actuaries 46: 99-191, 1994.

[26] W. Hackbusch, *A sparse matrix arithmetic base on $\mathcal{H}$-matrics. I. Introduction to $\mathcal{H}$-matrices,* Computing, 62: 89-108, 1999.

[27] E. Hairer, K. Wanner, *Solving ordinary differential equations. Vol. 2. Stiff and differential-algebraic problems.* Springer Verlag, Heidelberg, 1996.

[28] E.G. Haug, J. Haug and A. Lewis, *Back to basics: a new approach to the discrete dividend problem,* Wilmott Magazine, 37-47, Sept 2003.

[29] J.C. Hull, *Options, futures and other derivatives,* Prentice-Hall Int. Inc, London, 1989.

[30] R. Kangro, R. Nicolaides. *Far field boundary conditions for Black-Scholes equations,* SIAM J. Numerical Analysis, 38(4): 1357-1368, 2000.

[31] S.G. Kou, *A jump diffusion model for option pricing,* Management Science, 48: 1086-1101, 2002.

[32] Y.K. Kwok, *Mathematical models of financial derivatives.* Springer Verlag, Heidelberg, 1998.

[33] A.L. Lewis, *A simple option formula for general jump-diffusion and other exponential Lévy processes,* 8th. Annual CAP Workshop on Derivative Securities and Risk Management, Nov. 2001.

[34] D. Madan and E. Seneta, *The v.g. model for share market returns,* Journal of Business 63: 511-524. 1990.

[35] D. Madan and F. Milne, *Option pricing with V. G. martingale components,* Mathematical Finance 1(4): 3955, 1991.

[36] D. Madan, P. Carr and E.C. Chang, *The variance gamma process and option pricing,* European Finance Review 2: 79105, 1998.

[37] R.C. Merton, *Option pricing when the underlying stocks are discontinuous,* J. Financ. Econ, 5: 125-144, 1976.

[38] G.H. Meyer, *Numerical investigation of early exercise in American puts with discrete dividends,* J. Comp. Finance, 5(2), Winter 2001/02.

[39] A.M. Matache, P.A. Nitsche and C. Schwab, *Wavelet Galerkin pricing of American options on Lévy Driven Assets,* Preprint.

[40] B. Øksendal, *Stochastic Differential Equations. An Introduction with Applications,* Springer-Verlag, Fifth edition, 2000.

[41] C.W. Oosterlee, *On multigrid for linear complementarity problems with application to American-style options,* Electr. Trans. on Num. Analysis, 15: 165–185, 2003.

[42] C.W. Oosterlee, C.C. Leentvaar and A. Almendral, *Pricing options with discrete dividends by high order finite differences and grid stretching,* in ECCOMAS 2004, P. Neittaanmäki, et al, eds. Proc. Jyväskylä, Finland, 24-28, 2004.

[43] P.A. Samuelson, *Rational theory of warrant pricing,* Indust. Management Rev. 6: 13-32, 1965.

[44] W. Schoutens, *The Meixner Process: Theory and Applications in Finance,* EURANDOM Report 2002-004, EURANDOM, Eindhoven, 2002.

[45] W. Schoutens, *Lévy processes in Finance,* Wiley, 2003.

[46] D. Tavella, C. Randall, *Pricing financial instruments, the finite difference method,* Wiley New York, 2000.

[47] C. Van Loan, *Computational frameworks for the fast Fourier transform,* vol. 10 of frontiers in Applied Mathematics, SIAM, Philadephia, 1992.

[48] C. Wallner and U. Wystrup, *Efficient computation of option price sensitivities for options of American style,* Wilmott Magazine 2-11, November 2004.

[49] P. Wilmott, S. Howison, J. Dewynne, *The mathematics of financial derivatives,* Cambridge University Press, Cambridge, 1997.